Research Square

Preprints are preliminary reports that have not undergone peer review.
They should not be considered conclusive, used to inform clinical practice,
or referenced by the media as validated information.

Controls on Diagenetic Evolution and Porosity Development in Alkaline Lacustrine Carbonates: Insights from the Aptian Barra Velha Formation (Pre-salt, Santos Basin, Brazil)

Andreas Pauli de Castro[1]

andreasgeologia@gmail.com

Universidade Federal do Rio de Janeiro

Jessica Oste[1]

Universidade Federal do Rio de Janeiro

Leonardo Borghi[1]

Universidade Federal do Rio de Janeiro

Research Article

Keywords:

Posted Date: November 24th, 2026

DOI: https://doi.org/10.21203/rs.3.rs-10458836/v1

License: This work is licensed under a Creative Commons Attribution 4.0 International License.
Read Full License

Additional Declarations: No competing interests reported.

Controls on Diagenetic Evolution and Porosity Development in Alkaline Lacustrine Carbonates: Insights from the Aptian Barra Velha Formation (Pre-salt, Santos Basin, Brazil)

Andreas Pauli de Castro[1]*, Jessica Oste[1], Leonardo Borghi[1]

[1] LAGESED, Department of Geology, Federal University of Rio de Janeiro, CCMN, Cidade Universitária, Rio de Janeiro, CEP 21941-916, Rio de Janeiro, Brazil

Abstract: Understanding the diagenetic evolution of alkaline lacustrine carbonate reservoirs is essential for predicting reservoir quality in heterogeneous depositional systems. The Aptian Barra Velha Formation, the principal pre-salt reservoir of the Santos Basin, displays marked lithological and diagenetic variability that strongly influences porosity evolution. This study investigates the diagenetic history of the Mero Field through an integrated petrographic analysis of 109 thin sections from core and sidewall samples using transmitted-light, cathodoluminescence, and fluorescence microscopy. The earliest diagenetic stages were characterized by recrystallization of primary Mg-rich calcite, replacement of magnesium-rich silicates by dolomite, and precipitation of calcite, dawsonite, and silica under alkaline conditions inherited from deposition. Partial dissolution of these phases generated secondary porosity, whereas mesodiagenesis was dominated by chemical compaction, stylolite development, pressure solution, and extensive silica remobilization along preferential fluid-flow pathways. During deep burial, fluid circulation promoted the precipitation of megaquartz, saddle dolomite, sulfates, and sulfides, accompanied by localized carbonate dissolution, consistent with hydrothermal fluid circulation. The results demonstrate that reservoir quality reflects the cumulative effects of early mineralogical composition, facies heterogeneity, burial-related fluid-rock interaction, and structural reactivation. These findings provide new insights into the controls on porosity evolution in the Barra Velha Formation while

contributing to broader conceptual models of fluid-rock interaction and reservoir quality evolution in alkaline lacustrine carbonate systems.

Key-words: Alkaline lacustrine carbonates; Dolomitization; Silicification; Fluid–rock interaction; Porosity evolution

1. Introduction

Diagenetic evolution exerts a fundamental control on the petrophysical properties of the Barra Velha Formation reservoirs, where dissolution, mineral replacement, compaction, and cementation extensively modified depositional fabrics and primary porosity (Basso et al. 2020; Menchick et al. 2026). Understanding these processes in pre-salt lacustrine carbonates remains challenging because of marked facies and mineralogical heterogeneity, the absence of suitable modern analogues, and unusual carbonate textures and magnesium silicates, which hinder predictive diagenetic models for continental carbonate reservoirs (Rebelo et al. 2023; Carvalho and Fernandez 2021).

Silicification, dolomitization, and dissolution are the principal diagenetic processes modifying the mineralogy and pore systems of the Barra Velha Formation and represent major controls on reservoir quality in alkaline lacustrine carbonates (Basso et al. 2020; Carvalho et al. 2022; Wang et al. 2023; Leite et al. 2025; Matheus et al. 2025; Cembrani et al. 2026). Despite advances in understanding the Aptian carbonates of the Santos Basin, the origin, composition, and circulation pathways of the fluids responsible for these transformations remain debated (e.g., Farias et al. 2019; Silva et al. 2025). Likewise, the influence of facies variability on diagenetic pathways and porosity evolution remains poorly constrained, particularly regarding how carbonate fabrics control mineral replacement, silicification, dissolution, and porosity preservation. This uncertainty limits

predictive models of reservoir heterogeneity in compositionally complex lacustrine carbonate systems.

The Aptian Barra Velha Formation is the principal carbonate reservoir of the Santos Basin pre-salt succession (Moreira et al. 2007; Rodríguez-Berriguete et al. 2022) and one of the most extensive alkaline lacustrine carbonate systems recorded during the Early Cretaceous. It comprises predominantly in situ lacustrine carbonates, including shrubstones, crystalline crusts, muddy-spherulitic limestones, and microbialites, associated with reworked intraclastic deposits, subordinate terrigenous sediments, and magnesium silicates formed under alkaline to hyperalkaline conditions (Wright and Barnett 2015; Farias et al. 2019; Terra et al. 2023; Silva et al. 2025; Castro et al. 2026). These environmental and mineralogical characteristics contributed to highly heterogeneous diagenetic pathways and pore systems.

The Mero Field provides an important opportunity to investigate the diagenetic evolution of the Barra Velha Formation. Although it is one of the largest producing fields in the Brazilian pre-salt province, characterized by thick hydrocarbon-bearing carbonate successions (ANP 2021), integrated petrographic studies addressing its diagenetic evolution remain scarce (e.g., Pozi et al. 2024). Constraining these processes is essential for refining reservoir-quality prediction in heterogeneous pre-salt carbonate reservoirs and advancing conceptual models of diagenetic evolution in alkaline lacustrine carbonate systems. This study aims to characterize the petrographic and mineralogical evolution of the Barra Velha Formation in the Mero Field, establish its paragenetic sequence, and evaluate the principal controls governing porosity evolution and reservoir heterogeneity.

2. Geological Setting

2.1 Formation of the Santos Basin

The Santos Basin is a polyphasic passive-margin basin located along the southeastern Brazilian continental margin, extending offshore of the states of Rio de Janeiro, São Paulo, Paraná, and Santa Catarina. It exhibits a predominant NE–SW structural trend and is bounded by the Cabo Frio High and Campos Basin to the north, and by the Florianópolis Platform and Pelotas Basin to the south (Milani et al. 2000; Cainelli and Mohriak 1999; Moreira et al. 2007; Chang et al. 2008) (Fig. 1A).

The basin originated during the Late Jurassic–Early Cretaceous breakup of Gondwana and opening of the South Atlantic Ocean, when extensional tectonics produced asymmetric horst-and-graben systems through the reactivation of Precambrian basement structures (Chang et al. 1992; Cainelli and Mohriak 1999; Davison 2007; Mohriak et al. 2008). These tectonic elements exert a primary control on the geometry and distribution of the sedimentary succession (Leite et al. 2025). Within this tectono-stratigraphic framework, the São Paulo Plateau comprises a region of hyperextended continental crust that includes the Santos Outer High (Gomes et al. 2002; Carminatti et al. 2008).

Recent studies interpret the Santos Basin as a hyperextended passive margin shaped by oblique rifting, crustal thinning, and long-lived structural inheritance, with its evolution influenced by both tectonic and thermal processes associated with South Atlantic opening and Mesozoic magmatism (Unternehr et al. 2010; Manzo et al. 2012; Gomes and Vasconcelos 2021; Corrêa et al. 2025; Leite et al. 2025).

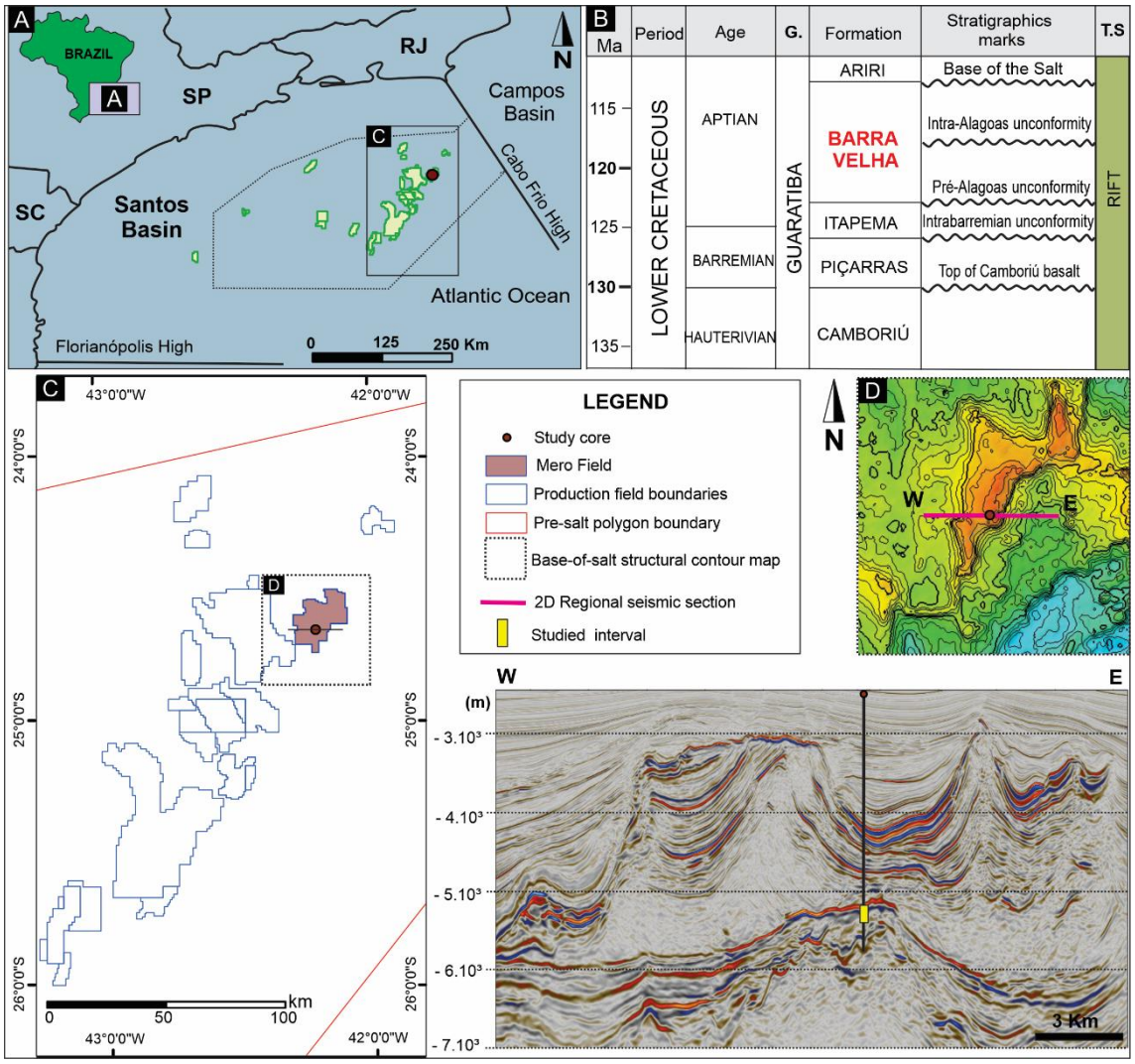

Figure 1 - Geological setting and stratigraphic framework of the studied interval. A) Location map of the Santos Basin. B) Chronostratigraphic framework of the Pre-salt succession in the Santos Basin. TS = tectonic setting; G = Group. C) Location of the studied well within the Mero Field. D) Structural contour map of the base of the salt (Ariri Formation) and W–E-oriented seismic section showing the position of the studied interval.

2.2 Stratigraphy of the Pre-Salt Interval of the Santos Basin

According to Moreira et al. (2007), the sedimentary succession comprises three tectonostratigraphic supersequences (rift, post-rift/sag, and drift), of which the rift and

post-rift/sag supersequences constitute the pre-salt interval. The rift stage begins with the tholeiitic basalts of the Camboriú Formation, followed by the lacustrine siliciclastic deposits of the Piçarras Formation, composed of sandstones, siltstones, shales, and polymictic conglomerates (Moreira et al. 2007; Carlotto et al. 2017; Brito et al. 2024; Marins et al. 2025). These units are overlain by the lacustrine carbonates of the Itapema Formation, consisting mainly of coquinas interbedded with organic-rich shales and locally affected by dolomitization and silicification. Its upper boundary is defined by the Pre-Alagoas Unconformity (Moreira et al. 2007; Rocha et al. 2021; De Jesus et al. 2023; Altenhofen et al. 2026).

The Eoaptian Barra Velha Formation is bounded by the Pre-Alagoas Unconformity at its base and by the erosional surface underlying the evaporites of the Ariri Formation at its top (Moreira et al. 2007; Alves et al. 2017; Gomes et al. 2020). Internally, the Intra-Alagoas Unconformity separates lower and upper intervals traditionally related to the rift and sag phases (Wright and Barnett 2015; Buckley et al. 2015; Adriano et al. 2022).

Although traditionally interpreted as recording the transition from syn-rift tectonism to thermal subsidence (Moreira et al. 2007), recent studies suggest deposition under continued tectonic activity, with fault reactivation and persistent structural control on sedimentation (Araújo et al. 2022; Terra et al. 2023; Leite et al. 2025; Silva et al. 2025). The Barra Velha Formation is dominated by in situ continental carbonates, including shrub-like limestones, crystalline crusts, muddy-spherulitic limestones, and microbialites, together with reworked intraclastic facies and minor siliciclastic input deposited in an alkaline lacustrine system (Farias et al. 2019; Gomes et al. 2020; Herlinger et al. 2023; Rebelo et al. 2023; Brito et al. 2024; Matheus et al. 2025; Castro et al. 2026).

2.3. Diagenetic Framework of the Barra Velha Formation

The Barra Velha Formation has undergone intense and spatially heterogeneous diagenetic alteration, producing distinct paragenetic assemblages and diagenetic phase associations across the pre-salt reservoirs (Carvalho et al. 2022; Leite et al. 2025; Menezes et al. 2025). These processes commonly overprint primary depositional characteristics, complicating the distinction between depositional and post-depositional features (Lima et al. 2020; Azaredo et al. 2021; Menchick et al. 2026). Eodiagenetic, mesodiagenetic, and hydrothermal stages have been recognized, with dolomitization, silicification, dissolution, and physical to chemical compaction representing the principal diagenetic processes. Compaction-related features include stylolites, fractures, and hydraulic breccias (Armelenti et al. 2016; Farias et al. 2019; Carvalho et al. 2022).

Dolomitization affects both in situ and reworked carbonate facies and records multiple episodes of precipitation, replacement, and cementation driven by lacustrine, diagenetic, and hydrothermal fluids (Herlinger et al. 2017; Farias et al. 2019; Azerêdo et al. 2021; Carvalho and Fernandez 2021). Silicification is similarly pervasive, occurring through replacement of carbonate phases and Mg-rich clay minerals, as well as pore- and fracture-filling cementation (Saller et al. 2016; Lima et al. 2020). Recent studies have further recognized early silicification associated with microbial activity and Mg-clay alteration, followed by late-stage silica redistribution controlled by fluid circulation along faults and fractures (Castro et al. 2026; Cembrani et al. 2026), emphasizing the strong mineralogical and petrophysical heterogeneity that characterizes the Barra Velha reservoirs.

3. Materials and Methods

This study is based on approximately 90 m of sampled interval from the Barra Velha Formation in the Mero Field (Fig. 1C–D). A total of 109 petrographic thin sections prepared from core samples and sidewall cores were analyzed. The thin sections were

impregnated with blue-dyed epoxy resin for porosity identification and subsequently stained with Alizarin Red S to discriminate carbonate phases. Petrographic analysis focused on identifying lithotypes, diagenetic products, and post-depositional processes affecting the unit. Lithological classification followed the scheme proposed by De Ros and Oliveira (2023), combined with the textural classifications of Dunham (1962) for carbonate rocks and Blair and McPherson (1999) for rudaceous deposits. Porosity classification followed the framework established by Choquette and Pray (1970).

Fluorescence microscopy was performed under blue (450–490 nm) and ultraviolet (365 nm) excitation using FS09 (FITC) and FS01 (DAPI) filters coupled to a Zeiss Imager A1 microscope. The technique was used to support the discrimination of diagenetic phases and to identify cementation, mineral replacement, recrystallization, microporosity, and mineralogical zoning (Dravis and Yurewicz 1985; Dravis 1991). Cathodoluminescence analyses were carried out using a CITL MK5-2 system coupled to a Zeiss Scope A1 microscope. This technique was used to distinguish primary and diagenetic phases and to identify mineral growth, dissolution, recrystallization, microfracturing, and replacement, supporting reconstruction of the paragenetic sequence and porosity evolution (Machel 2000; Pagel et al. 2000; Hiatt and Pufahl 2014).

4. Results

4.1. Lithotypes and Petrographic Characteristics

The studied interval is dominated by in situ carbonate lithotypes, mainly represented by spherulestones (24%), shrubstones (17%), and microbialites (16%). Intraclastic lithotypes, including calcarenites and calcirudites, account for approximately 30% of the samples, whereas mudstones represent 8% (Fig. 2). Cherts and dolostones comprise approximately 5% and are strongly affected by diagenetic alteration, commonly

obliterating primary depositional fabrics. All lithotypes display variable degrees of mineral replacement, recrystallization, cementation, and dissolution, which influence the preservation of depositional textures. The main petrographic characteristics of each lithotype are described below.

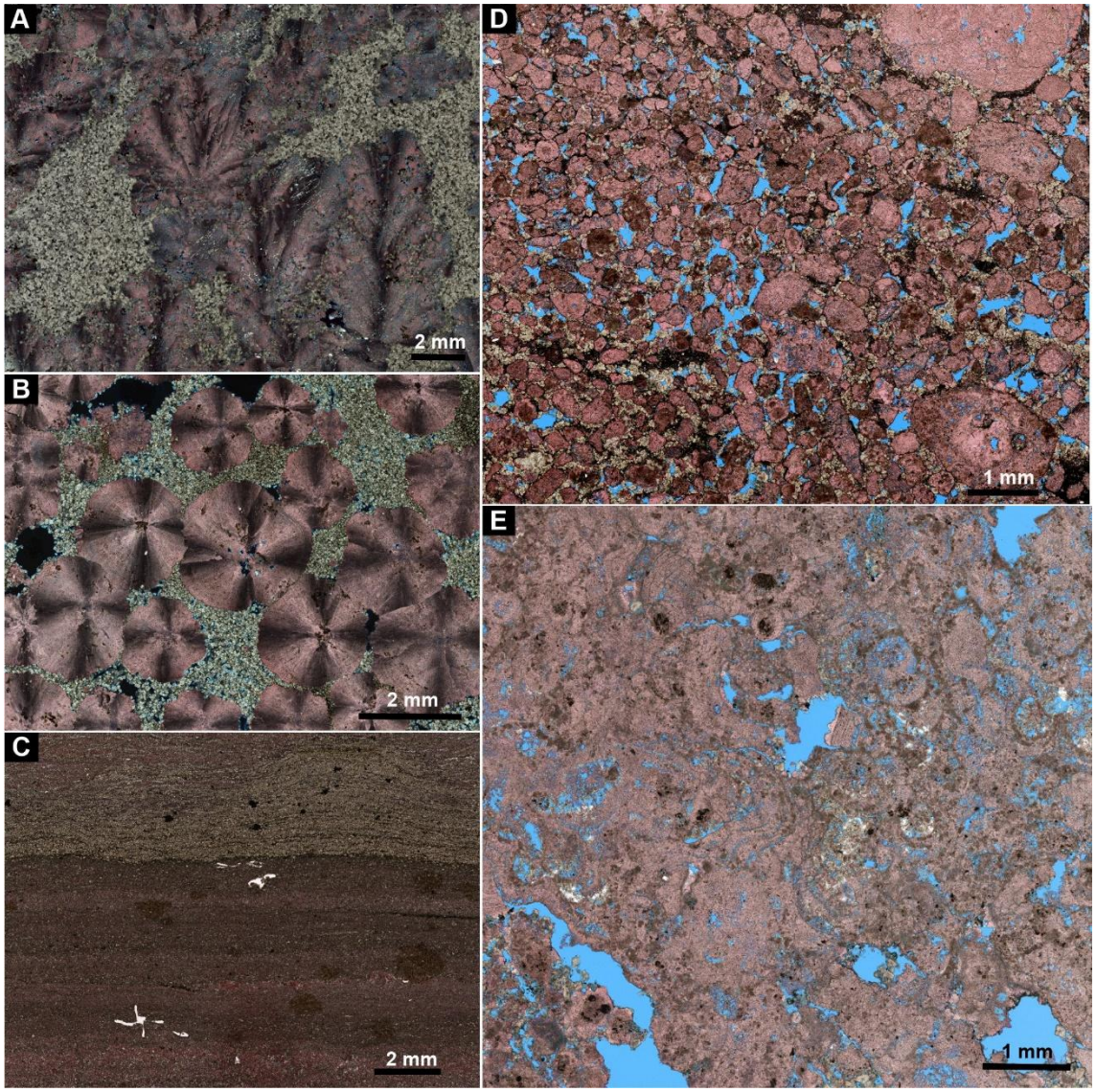

Figure 2 - Lithotypes micrography of the studied interval. A) Shrubstone composed of arborescent shrubs with fascicular-optic texture, embedded in a dolomitized interparticle matrix. B) Spherulitestone composed of fibrous-radial calcitic spherulites within a blocky dolomite matrix. C) Mudstone displaying planar lamination defined by the interbedding of microcrystalline calcite and dolomitized layers. D) Framework-supported intraclastic calcarenite characterized by coarse-sand-sized grains and predominantly rounded to well-

rounded intraclasts. E) Microbialite exhibiting thrombolitic fabric and microsparitic to peloidal texture.

4.1.1 Shrubstones

Shrubstones consist of limestones dominated by in situ calcitic shrubs with arborescent morphologies and subordinate dendritic to columnar forms. Shrub elements commonly display fascicular-optic textures, forming partially coalescent frameworks or, locally, loosely arranged fabrics (Fig. 2A). The shrubstones display a stratified structure defined by the planar superposition of shrub elements, forming intervals with variable packing density. Interparticle spaces locally preserve primary carbonate fragments, spherulites, and dispersed Mg- and K-rich clay minerals.

Interparticle dolomite occurs predominantly as loosely distributed blocky dolomite and, secondarily, as coalesced dolomite. Micro- to macrocrystalline quartz and chalcedony are common, whereas barite, celestine, and pyrite locally occur, filling secondary pores and fractures. Diagenetic alteration includes intraparticle dissolution, chemical compaction marked by stylolites and dissolution seams, and partial replacement by dolomite and silica. The reduced abundance of depositional matrix favors the predominance of intershrub growth-framework porosity.

4.1.2 Spherulestones

The spherulestones correspond to limestones composed of calcitic spherulites immersed in a matrix of magnesium-rich clay minerals or replacive dolomite, including muddy spherulitestones, spherulitestones, and spherulitic mudstones (Fig. 2B). These lithotypes are mainly matrix-supported, with fine sand- to granule-sized spherulites displaying spherical to irregular morphologies, fibro-radial textures, and locally weak

concentric lamination. Subordinate framework-supported intervals are also observed, in which the spherulites display punctual to sutured contacts. Peloidal nuclei and clay-mineral inclusions are common, whereas calcispheres, ostracods, phosphatic fossils, and rare fine-grained siliciclastic components occur subordinately.

Partial dissolution of the spherulites is recurrent, preferentially affecting their nuclei. Post-depositional alteration comprises pervasive dolomite replacement of the depositional matrix, subordinate silica replacement locally extending into the spherulitic framework, dissolution seams and stylolites, and cementation by micro- to macrocrystalline quartz and chalcedony. Barite, celestine, and pyrite locally fill pores and fractures, whereas dawsonite occurs within interparticle spaces.

4.1.3 Mudstones

The mudstones are composed of millimeter-scale calcitic crusts, predominantly tabular, locally laminated, and displaying micro-sparitic textures, interlayered with replacive dolomite levels, mainly characterized by blocky to mosaic textures (Fig. 2C). The dolomite commonly exhibits turbid cores associated with remnants of magnesium-rich clay minerals. The intercalation of peloidal clay-rich laminae, calcitic crusts, and dolomitized intervals imparts a planar- to wavy-parallel lamination to the lithotype. Subordinate discontinuous lenticular levels of microsparitic calcite also occur.

Articulated ostracods, phosphatic fragments, and fine siliciclastic grains, including quartz, feldspars, and clay minerals, are common and frequently aligned parallel to the lamination. Deformational structures, such as irregular fractures and faults, are recurrent, and silicification locally promotes deformation and displacement of the lamination. Porosity is predominantly fracture-related and, subordinately, vuggy.

4.1.4 Clastic Lithotypes

The intraclastic lithotypes comprise calcarenites, calcirudites, and sedimentary breccias of predominantly carbonate composition, with subordinate hybrid sandstones (Fig. 2D). The framework is mainly composed of reworked fragments of shrubstones, spherulestones, microbialites, peloids, ostracods, phosphatic fossils, and undifferentiated carbonate clasts, with minor siliciclastic grains including quartz, chert, feldspar, muscovite, and clay minerals.

These lithotypes are predominantly framework-supported and display variable textural maturity. Calcirudites and breccias are poorly sorted and dominated by subangular to subrounded fragments, whereas calcarenites show better sorting and more rounded grains. Grain contacts range from planar to sutured.

The main diagenetic features include interparticle dolomitization, silicification, and subordinate calcitic cementation. Micro- to macrocrystalline quartz and chalcedony occur as pore-filling cements and replace primary components, whereas calcite cement locally occupies residual primary porosity. Grain fracturing, chemical compaction represented by stylolites, and partial dissolution of intraclastic components are common. The low abundance of depositional matrix favors interparticle porosity, with subordinate intraparticle, vuggy, and fracture-related porosity.

4.1.5 Microbialites

Microbialites include columnar microstromatolites, thrombolites, thrombo-pisolites, microbial mats, and reticulated fabrics, as described by Castro et al. (2026). They are predominantly composed of micro-sparitic calcitic components displaying peloidal to micropeloidal textures, including pisoids, oncoids, laminated columnar forms, and peloidal aggregates. Subordinate constituents include phosphatic fossils, framboidal pyrite, fine siliciclastic grains, bioclasts, and dispersed organic matter (Figure 2E).

The microbialites exhibit diagenetic modification, mainly marked by dolomitization, silicification, and recrystallization. Interparticle spaces are predominantly composed of blocky to mosaic dolomite, commonly zoned and locally impregnated by bitumen, whereas silica occurs as micro- to macrocrystalline quartz and chalcedony filling inter- and intraparticle porosity, fenestral pores, and locally replacing framework components. Subordinate discontinuous calcite fringes occur coating particles and pore margins. Barite is an accessory and locally occurs, filling secondary porosity.

4.2. Diagenetic products and processes

4.2.1. Calcite

Calcite commonly exhibits multiple stages of recrystallization, resulting in microsparitic to sparitic textures and locally producing fascicular-optic and crystalline mosaic fabrics (Fig. 3A–B). Calcite cement partially to completely occludes primary porosity and, locally, secondary porosity, including moldic and intraparticle pores (Fig. 3C). Calcite occurs as blocky to mosaic spar cement, isolated rhombohedral crystals, and discontinuous bladed fringes with spearhead-like morphologies (Fig. 3D). Locally, calcite forms isopachous prismatic cement growing from pore margins toward pore centers. Where present, microcrystalline dolomite rims coating framework grains are consistently overgrown by bladed calcite fringes (Fig. 3E). No evidence of dolomite rims overgrowing calcite cement was observed.

The crystals are generally clear and may engulf replacive dolomite. Locally, secondary dolomite is partially replaced by calcite, indicating episodes of dedolomitization (Fig. 3F). Calcite fringes are most common in microbialites and dendritic shrubstones, where they are associated with well-developed interparticle porosity. Sparry calcite cement occurs in shrubstones, microbialites, and spherulitestones.

Under cathodoluminescence, recrystallized calcite displays yellow to yellow-orange luminescence, whereas calcite cement exhibits yellow-orange to brownish-orange colors, commonly with internal zoning (Fig. 3G). Under fluorescence microscopy, calcite is non-fluorescent to weakly fluorescent, typically displaying dark-brown tones.

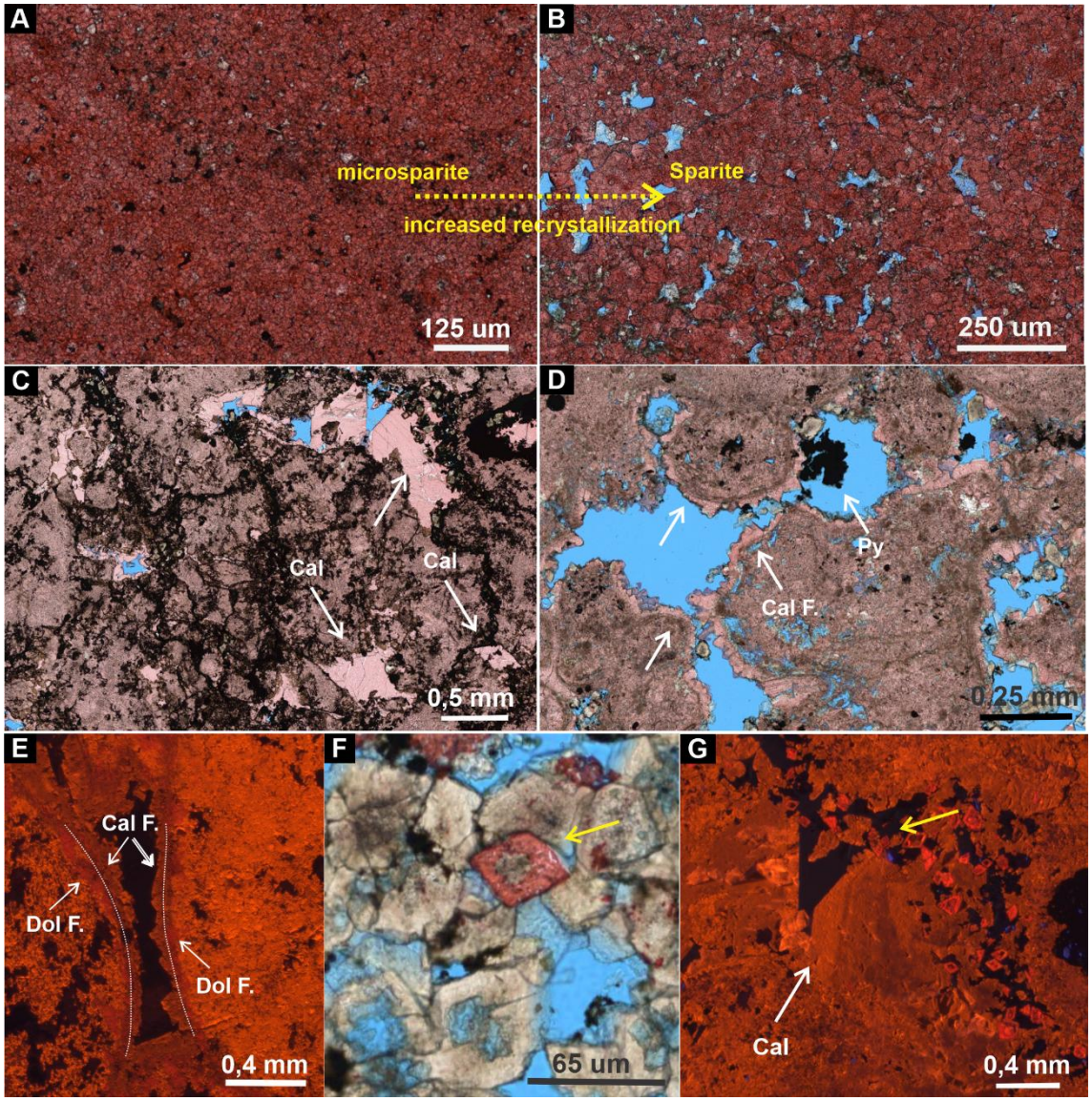

Figure 3 – Diagenetic calcite micrographs. (A–B) showing progressive recrystallization of primary calcite, marked by crystal coarsening from microsparite to sparite. (C) Sparry calcite cement partially occluding pore space. (D) Discontinuous and irregular bladed calcite fringes with dogtooth morphology. (E) Dogtooth calcite fringe overgrowing a microcrystalline dolomite rim surrounding a calcitic spherulite. (F) Replacive dolomite

crystals exhibiting partial calcite replacement (dedolomitization) and internal dissolution. (G) Calcite cement displaying compositional zoning under cathodoluminescence.

4.2.2. Dolomite

Dolomitization represents the most pervasive diagenetic phase within the studied interval. Dolomite occurs as a replacive phase affecting both matrix and framework components, as well as pore-filling cement (Fig. 4). In intensely dolomitized lithotypes, particularly where stylolites are absent, other diagenetic phases are generally poorly expressed. Four dolomite types were identified: microcrystalline dolomite, blocky dolomite, mosaic dolomite, and saddle dolomite.

Microcrystalline replacive dolomite is composed of anhedral crystals that locally preserve relics of the original fabric of the replaced components (Fig. 4A-B). Crystals may be either clear or turbid and commonly contain fluid inclusions. This phase occurs predominantly in shrubstones and spherulitestones and may be associated with mosaic dolomite.

Blocky dolomite occurs as dense aggregates or dispersed floating crystals, commonly controlling intercrystalline porosity. It consists of inequigranular subhedral to euhedral crystals with variable sizes (Fig. 4C). Remnants of primary Mg-clay minerals are commonly associated with blocky dolomite, and pyrite frequently occurs within the same domains (Fig. 4D). Internal zoning, darkened cores, partial dissolution associated with intracrystalline porosity, and bitumen impregnation are recurrent features (Fig. 4C).

Mosaic dolomite occurs mainly within interparticle spaces, particularly in spherulitestones. It consists of subhedral to anhedral crystals commonly characterized by turbid cores and planar to lobate intercrystalline contacts. Locally, bitumen-filled

intercrystalline porosity is developed (Fig. 4E). Gradational transitions between blocky and mosaic dolomite are common and generally marked by progressive changes in crystal size and habit (Fig. 4F).

Dolomite cement occurs mainly as a vug- and fracture-filling saddle dolomite phase. It consists of coarse, clear crystals with curved crystal faces and undulose extinction, locally displaying internal zoning, and is frequently associated with barite and celestine. More rarely, a thin fringe of microcrystalline dolomite surrounds spherulites and intraclastic grains, forming continuous coatings around particles with corroded margins (Fig. 4G).

Under cathodoluminescence, dolomite predominantly exhibits red luminescence, and zoned crystals with bands ranging from red to brownish red are common (Fig. 4H). Non-zoned crystals also occur, displaying colors ranging from reddish orange and intense blood-red to reddish-brown tones (Fig. 4B). Under fluorescence microscopy, dolomite is weakly fluorescent, typically exhibiting brown to brownish-orange hues.

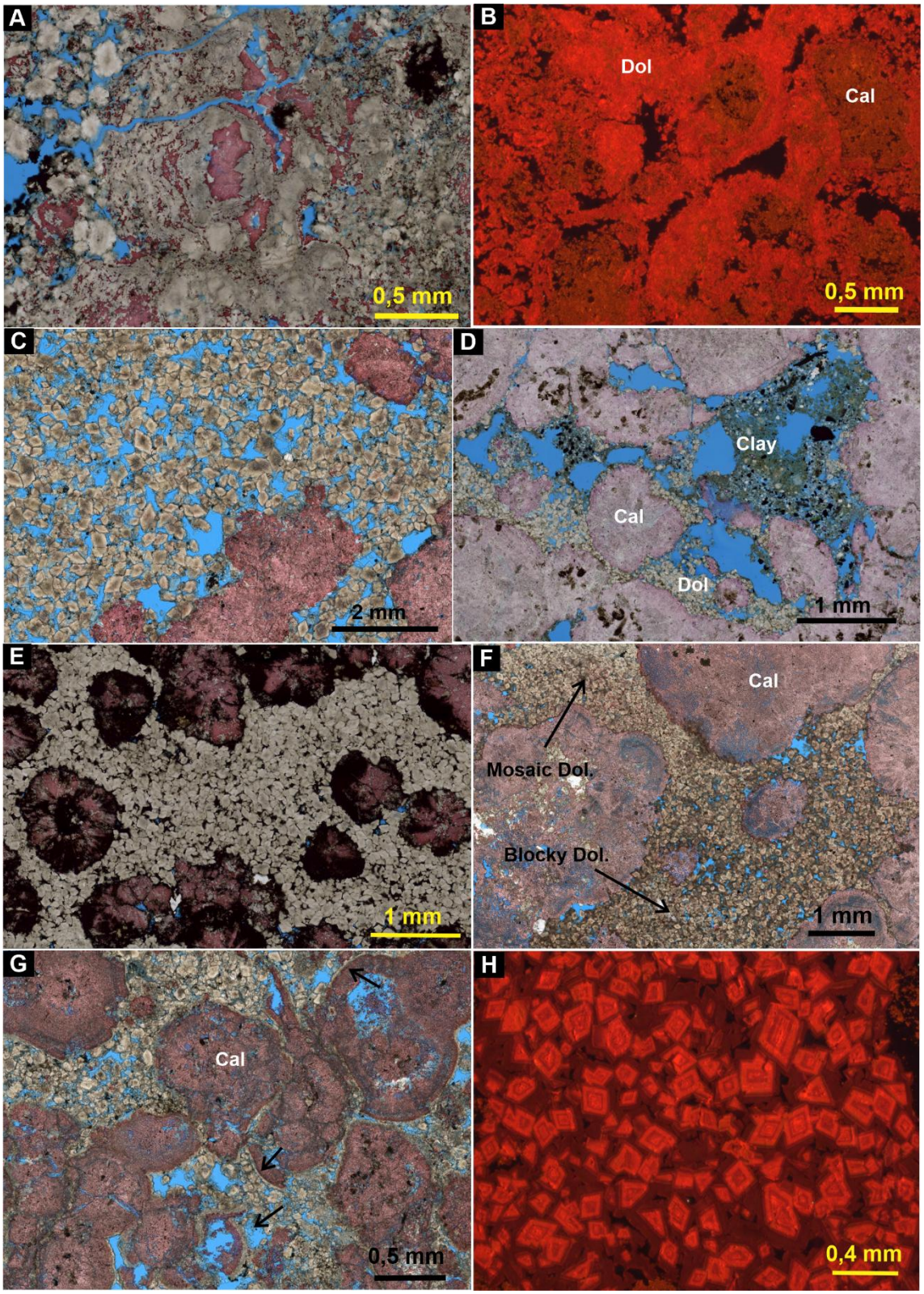

Figure 4 – Dolomite types and dolomitization features. A–B) Microcrystalline replacive dolomite affecting calcitic framework components and dense blocky dolomite occupying interparticle pore space, under transmitted light (PPL) and cathodoluminescence, respectively. C) Floating blocky dolomite characterized by turbid crystal cores. D)

Replacive dolomite associated with relics of primary magnesium-rich clay minerals preserved within the interparticle domain. E) Mosaic dolomite exhibiting bitumen-filled intercrystalline porosity. F) Gradational transition between dense blocky and mosaic dolomite, accompanied by progressive reduction in crystal size and intercrystalline porosity. G) Microcrystalline dolomite rim coating framework particles (black arrow), followed by precipitation of interparticle blocky dolomite cement. H) Subhedral to euhedral rhombohedral dolomite crystals displaying compositional zoning under cathodoluminescence.

4.2.3. Silica

Silica occurs both as a replacive phase affecting primary constituents and as a pore-filling cement, representing the most abundant cementing phase within the studied interval (Fig. 5A). Intense silicification commonly occurs adjacent to stylolitic zones and is frequently confined between stylolites or dissolution seams. Under cathodoluminescence, silica is generally weakly luminescent to non-luminescent, with localized dark-blue to violet responses. Under fluorescence microscopy, silica is predominantly non-fluorescent.

Macrocrystalline mosaic silica occurs exclusively as cement, filling interparticle, intraparticle, vuggy, and fracture porosity (Fig. 5B). It consists of clear subhedral to anhedral crystals and, subordinately, euhedral prismatic crystals, locally exhibiting internal zoning and fluid inclusions. Silica commonly engulfs calcite and dolomite crystals, with polygonal to serrated intercrystalline contacts, locally displaying undulose extinction and oriented crystal growth, particularly in vein-related occurrences.

Microcrystalline silica occurs replacing framework (e.g., spherulites, intraclast grains, bioclasts) and matrix components (e.g, Mg-clay minerals), while also filling pore space (Fig. 5A). It consists of anhedral crystals displaying predominantly serrated to dentate intercrystalline contacts. It is commonly associated with chalcedony and, subordinately, with macrocrystalline quartz. In some cases, transitions between these phases are abrupt and marked by the concentration of bitumen along crystal boundaries.

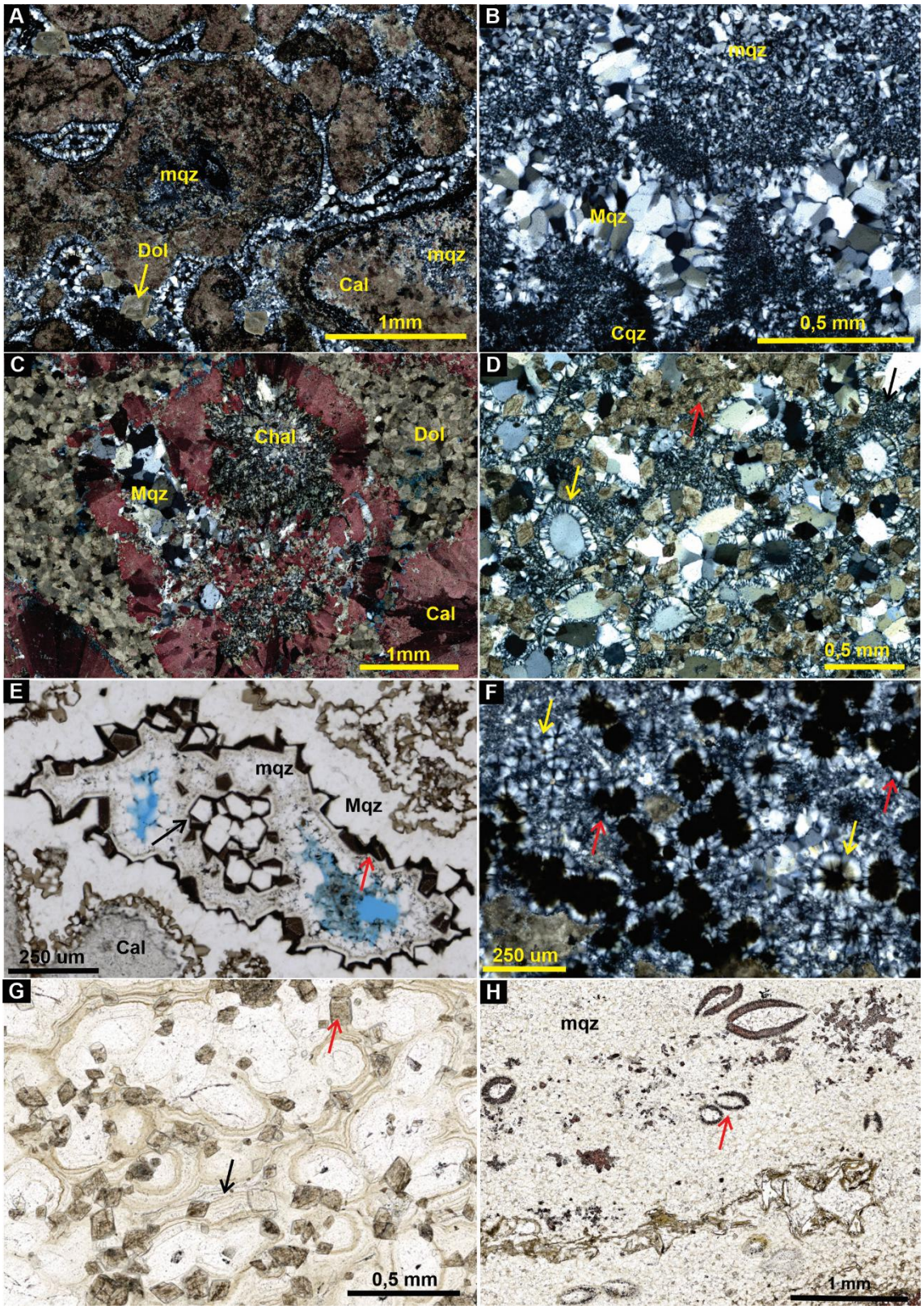

Figure 5 – Diagenetic silica phases. A) Intensely silicified calcarenite showing framework replacement and intergranular pore-filling silica cement. B) Association of macrocrystalline quartz (Qtz), microcrystalline quartz (qtz), and cryptocrystalline silica (Cqz). C) Calcitic spherulite replaced by fibrous-radial chalcedony, with intraparticle

porosity filled by megaquartz cement. D) Framework grains displaying one or more generations of drusy and comb quartz cement (yellow arrow) developed along serrated to sutured grain contacts. Intergranular pore space is filled by microcrystalline quartz and subordinate chalcedony (black arrow). E) Association of multiple silicification phases, including alternating microcrystalline and macrocrystalline quartz with anhedral and euhedral-prismatic habits, respectively, filling vugular porosity. F) Spherulitic chalcedony associated with bitumen impregnation. G) Banded chert showing multiple silica phases and dispersed rhombohedral dolomite crystals. H) Chert with extensive replacement of the primary fabric by microcrystalline silica, preserving relic calcitic ostracods and phosphatic fossils (red arrow).

Chalcedony occurs both as a replacive phase affecting framework particles and as a cement partially to completely filling intraparticle porosity, displaying characteristic fibrous-radial textures (Fig. 5C). When replacive, it commonly preserves the original textural orientation of the replaced components. As a cement, chalcedony is typically associated with micro- and macrocrystalline quartz and, subordinately, with celestine. Hydrocarbon-associated microporosity is common, and silicification locally preserves residual carbonate cores surrounded by replacive silica halos. Laminated particles, including shrubs, pisoids, and oncoids, commonly exhibit infilling by microcrystalline silica and chalcedony along internal discontinuities.

Drusy and comb quartz cements occur mainly in hybrid sandstones and commonly display a palisade habit, growing from grain surfaces toward pore centers until complete pore occlusion (Fig. 5D). These cements may represent multiple growth stages or a single generation of elongated crystals. They commonly exhibit irregular to sutured contacts

with framework grains. Thin, discontinuous syntaxial overgrowths are also locally developed.

Less common silica phases include cryptocrystalline silica, botryoidal quartz, and spheroidal quartz. Cryptocrystalline silica occurs mainly in microbialites and intensely silicified spherulitestones and displays orange to brownish-orange fluorescence under fluorescence microscopy. Botryoidal quartz exhibits characteristic banding produced by the alternation of micro- and macrocrystalline silica (Fig. 5E). Spherulitic chalcedony, characterized by fibroradial textures, is commonly associated with bitumen impregnation (Fig. 5F).

In cherts, pervasive silicification results in the partial to complete obliteration of primary depositional features (Fig. 5G). These lithotypes are composed predominantly of micro- to macrocrystalline quartz containing euhedral to rhombohedral dolomite crystals characterized by internal compositional zoning and turbid cores. Late-stage hydrocarbon-filled fractures are common. More rarely, flower-shaped silica spherulites occur without evidence of pre-existing carbonate spherulites, together with replacement of carbonate components, including ostracods and phosphatic fossils (Fig. 5H).

4.2.4. Accessory Minerals

Celestine predominantly exhibits a fibrous habit and commonly occurs in association with microcrystalline silica, chalcedony, and barite (Fig. 6A). Pyrite occurs mainly as aggregates of subhedral to anhedral crystals and, subordinately, as isolated cubic crystals filling secondary porosity. Framboidal pyrite is common in microbialites, where it is typically associated with organic matter and, locally, with remnants of the magnesium clay-rich matrix. In general, pyrite occurs either as a pore-filling phase or associated with replacive dolomite (Fig. 6B).

Dawsonite occurs exclusively in shrubstones and spherulitestones, where it fills interparticle pores associated with preserved Mg-rich clay minerals. It forms aggregates of euhedral acicular crystals with divergent radial growth and locally contains dark inclusions resembling the adjacent clay-rich matrix (Fig. 6C). Barite occurs as predominantly tabular subhedral to euhedral crystals filling interparticle and vugular porosity and, less commonly, intraparticle pores (Fig. 6D). Crystals are typically coarse, locally exceeding 2 mm in size, and commonly contain rhombohedral dolomite and fluid inclusions.

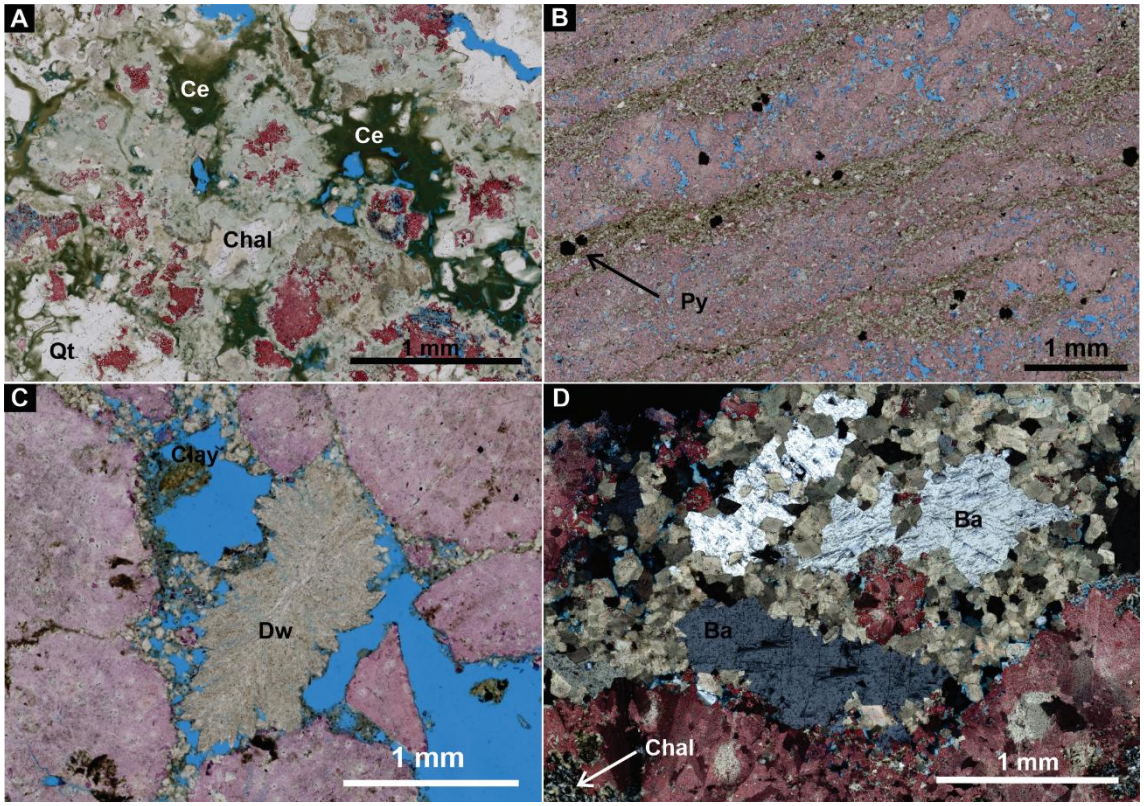

Figure 6 – Accessory mineral phases. A) Association of celestine (Cel), macrocrystalline quartz (Qtz), and chalcedony (Chal) filling interparticle porosity. B) Subhedral pyrite crystals concentrated within dolomitized intervals. C) Fibrous dawsonite (Dw) crystal exhibiting divergent plume-like growth and filling interparticle porosity in a shrubby spherulitestone, associated with relic primary magnesium-rich clay minerals and dolomite. D) Large subhedral to anhedral barite crystals associated with mosaic and

rhombohedral dolomite. Dolomite occurs both enclosing barite crystals and as inclusions within barite.

4.3. Compaction and Porosity System

Mechanical compaction features include planar to concavo-convex contacts between particles, fracturing of framework components (e.g., bioclasts, phosphatic fossils, and carbonate intraclasts), and deformation of ductile constituents such as peloids and clay minerals (Fig. 7A). Chemical compaction is equally pervasive and is expressed by lobate and sutured contacts, dissolution seams, and stylolites displaying a variety of geometries, including anastomosing, suture, sharp-peak, and long-parallel morphologies (sensu Koehn et al. 2016; Fig. 7B). Stylolites commonly crosscut both framework particles and matrix and may be filled by bitumen and clay minerals (Fig. 7C). Quartz grains also record evidence of chemical compaction, including pressure dissolution and the development of lobate and sutured contacts (Fig. 7D).

Dissolution constitutes one of the principal processes responsible for the generation and modification of secondary porosity (Fig. 7E). Intraparticle dissolution is recurrent, whereas complete removal of framework components results in moldic porosity. In spherulites and laminated shrubs, dissolution preferentially affects micritic to micropeloidal domains, corresponding to spherulite nuclei and internal shrub laminae, respectively (Fig 7F). In dolomite, dissolution is commonly selective and concentrated within crystal cores or along specific growth-zoning bands (Fig. 3F).

Porosity distribution varies significantly among lithotypes. In microbialites, fenestral, vuggy, intraparticle, and interparticle porosity predominate in decreasing order of abundance (Fig. 7 E–F). Calcarenites and calcirudites are characterized predominantly by interparticle porosity, subordinately associated with intraparticle, vuggy, and fracture

porosity (Fig. 2D). Mudstones are dominated by fracture porosity, with subordinate vuggy and moldic pores. In spherulitestones, intra- and interparticle porosity constitute the dominant pore types (Fig, 7E).

In shrubstones, intershrub porosity is commonly enhanced by secondary dissolution. Growth-framework porosity is also widespread, occurring predominantly as intershrub growth-framework porosity and, subordinately, as interlaminar and intrashrub growth-framework porosity. Intercrystalline porosity is common within dolomitized domains, whereas intracrystalline microporosity occurs mainly in association with chalcedony (Fig. 4D).

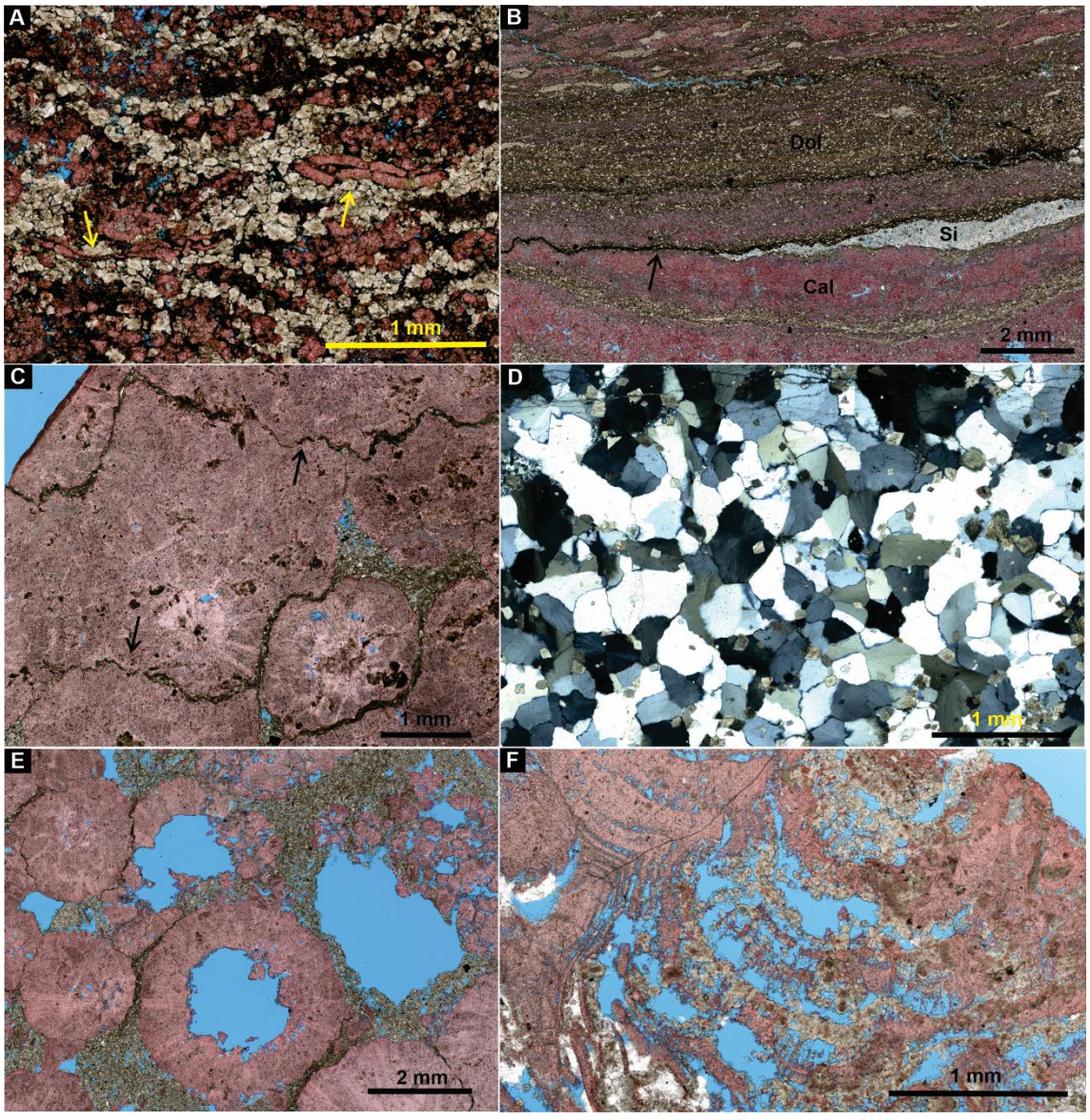

Figure 7 – Compaction features and pore-system characteristics. A) Deformed and fractured ostracod fragments (yellow arrow), illustrating mechanical compaction. B) Stylolite developed within a mudstone, associated with adjacent silicification. C) Sutured to stylolitic contacts between carbonate particles. D) Lobate to sutured grain contacts and undulose to sweeping extinction in quartz grains, indicating pressure-solution processes. E) Intraparticle porosity within spherulites associated with vugular and interparticle porosity. F) Fenestral and intraparticle porosity in microbialites.

5. Discussion

5.1. Paragenetic evolution

5.1.1 Calcite

Calcite is the dominant carbonate phase in the Barra Velha Formation, forming both syndepositional components (e.g., shrubs, oncoids, bioclasts, and intraclasts) and early diagenetic products, including spherulites (Fig. 2; Wright and Barnett 2015). Its diagenetic evolution reflects progressive modification from eodiagenetic conditions to deep burial stages (Saller et al. 2016; Mercedes-Martín et al. 2019; Lima et al. 2020; Brito et al. 2024).

Calcite spherulites are interpreted as products of early calcite precipitation during the initial stages of diagenesis (Tosca and Wright 2015; Wright and Barnett 2015; Herlinger et al. 2017), rather than primary depositional particles (Mercedes-Martín et al. 2017; Kirkham and Tucker 2018). Magnesian clay mineral inclusions within the spherulites indicate a close genetic association with Mg-silicate precursors, suggesting formation under syndepositional to earliest eodiagenetic conditions (Figs. 4D and 7C). In addition, partial obliteration of the spherulitic fabric by early dolomitization demonstrates

that spherulites were already present prior to or during the earliest diagenetic stages, reinforcing their formation in unconsolidated sediments.

During early diagenesis, the compositional instability of primary Mg-rich calcite promoted its recrystallization to low-Mg calcite (Saller et al. 2016; Altenhofen et al. 2024; Gomes et al. 2025), producing predominantly microsparitic to sparitic recrystallized calcite and locally preserving remnants of the primary depositional textures. (Fig. 3A – B; Farias et al. 2019).

Recrystallization proceeded mainly through fabric-retentive replacement, preserving precursor morphology while generating abundant microporosity and incorporating widespread mineral inclusions (Herlinger et al. 2017; Carvalho et al. 2022; Schrank et al. 2024). The degree of recrystallization reflects heterogeneities in early diagenetic fluid evolution, likely linked to variations in lacustrine water chemistry controlled by paleoclimatic oscillations affecting evaporation and meteoric–groundwater balance (Rebelo et al. 2023; Silva et al. 2025; Castro et al. 2026).

During mesodiagenesis, progressive neomorphism resulted in crystal coarsening and reorganization of carbonate fabrics during burial (Lima et al. 2020). At more advanced stages, recrystallization may be enhanced by the circulation of elevated-temperature basinal fluids, resulting in partial to complete obliteration of primary depositional fabrics (Tritlla et al. 2018). More porous and permeable facies, such as shrubstones and spherulitestones, were preferentially affected, indicating strong facies control on the distribution and intensity of diagenetic modification (Brito et al. 2024).

The intensification of these processes is commonly associated with tectonic reactivation and regional magmatism, which may have enhanced fluid circulation and thermal perturbations in the basin (Rochelle-Bates et al. 2022; Cembrani et al. 2026). In

some cases, intense calcite recrystallization has been attributed to thermal anomalies related to basic igneous intrusions (Marins et al. 2025).

Calcite cementation represents a multiphase process that contributes significantly to reservoir heterogeneity within the Barra Velha Formation (Fig. 3C; Carvalho et al. 2022; Matheus et al. 2025; Menchick et al. 2026). Early diagenetic cementation occludes primary porosity through the precipitation of discontinuous isopachous to tooth-like calcite fringes and pore-filling sparry calcite cement (Fig. 3D), as well as by the infilling of shrinkage pores associated with desiccation of magnesium-silicate gels (Carramal et al. 2022).

In contrast, mesodiagenetic stages are characterized by prismatic, blocky, and granular mosaic calcite cements filling faults, tectonic breccias, and secondary porosity (Fig. 3G; Lima et al. 2020; Carvalho and Fernandez 2021; Schrank et al. 2024; Corrêa et al. 2025; Menchick et al. 2026). These cements reflect precipitation from evolved basinal fluids during burial, with enhanced fluid flow along structurally controlled pathways. Subordinately, calcite also occurs infilling pore spaces generated by the dissolution of magnesium clay minerals (Herlinger et al. 2017).

5.1.2 Dolomite

Dolomite represents an abundant diagenetic phase within the Barra Velha Formation and occurs in a wide range of textural and morphological forms (Basso et al. 2020; Carvalho and Fernandez 2021). It predominantly replaces the primary Mg-silicate matrix and, subordinately, framework components, while also locally occluding pore space (Fig. 4). Several mechanisms have been proposed for its origin, including microbial precipitation, direct formation within the water column, hydrothermal fluid circulation, and pedogenic processes (Farias et al. 2019; Araújo et al. 2022; Carvalho et al. 2022;

Jácomo et al. 2023; Rebelo et al. 2023). The petrographic relationships observed in this study support an eodiagenetic origin for the dominant dolomitization phase through the alteration of magnesium clay minerals.

This interpretation is supported by the recurrent occurrence of turbid crystal cores rich in clay inclusions and remnants of magnesium silicates preserved within the dolomitic replacement matrix (Fig. 4C – D), indicating a close genetic relationship between dolomitization and the dissolution of unstable magnesium clay minerals (Wright and Barnett 2015; Menezes et al. 2025). Nevertheless, Rochelle-Bates et al. (2022) proposed that a significant proportion of dolomitization developed during later diagenetic stages, associated with the hydrothermal destabilization of these clay minerals during deep burial.

The distribution of replacive dolomite exhibits a strong facies control, being particularly abundant in spherulitestones and mudstones, facies originally enriched in primary clay minerals. In contrast, intraclastic limestones contain comparatively lower dolomite abundances (Fig. 2D), reflecting depositional conditions in which higher-energy processes favored the removal of the fine-grained clay fraction.

Replacive dolomite occurs predominantly as floating blocky dolomite, dense blocky dolomite, and mosaic dolomite, reflecting progressive degrees of replacement, with subordinate crystal reorganization during burial (Carvalho et al. 2022).

Dispersed blocky dolomite is interpreted as an early eodiagenetic phase resulting from the partial replacement of magnesium clay minerals, such as stevensite and kerolite, prior to significant compaction. Subsequent dissolution of these clay minerals generated secondary porosity (Fig. 4C), imparting an apparently “floating” character to the dolomite

rhombs within the pore system (Herlinger et al. 2023; Gomes et al. 2025; Altenhofen et al. 2024).

In contrast, dense blocky dolomite reflects pervasive dolomitization involving extensive replacement of the Mg-silicate matrix and progressive obliteration of the original depositional fabric. Mosaic dolomite is associated with more advanced diagenetic stages, characterized by continued replacement, with subordinate recrystallization and cementation under mesodiagenetic conditions, with possible overprint by elevated-temperature fluids during burial. The presence of sutured and lobate intercrystalline contacts (Fig. 6D), indicative of pressure dissolution, further supports formation under elevated burial depths and temperatures (Leite et al. 2025).

Gradational transitions between dense blocky and mosaic dolomite, together with their commonly turbid crystal cores and relatively clearer rims, dark-red to reddish-brown cathodoluminescence, preservation of relics of earlier textural phases, progressive reorganization of crystal fabrics, and systematic change in crystal size (Fig. 4F), represent successive stages of a replacement-dominated dolomitization pathway, with progressive recrystallization during burial.

Subordinate dolomite phases include saddle dolomite and thin dolomite fringes around spherulitic grains (Fig. 4G). Saddle dolomite occurs in fractures, vugs, and fault-related zones and is commonly associated with barite, celestine, and pyrite. This assemblage indicates precipitation from warm basinal brines during late mesodiagenesis to deep burial conditions, with possible localized input of higher-temperature, hydrothermal-derived fluids along fault zones (Herlinger et al. 2017; Carvalho et al. 2022; Lima et al. 2020; Brito et al. 2024).

Dolomite fringes have been reported in the Barra Velha Formation and correlative units, such as the Macabu Formation (Basso et al. 2020; Azerêdo et al. 2021; Lima et al. 2020). These features are commonly interpreted as the product of replacement of magnesium clay mineral coatings that originally surrounded framework grains (Wright and Barnett 2020; Carramal et al. 2022), although they may also reflect early eodiagenetic precipitation or the replacement of pre-existing calcite cements (Azerêdo et al. 2021). Their preferential occurrence around spherulites suggests a strong control exerted by the alteration of magnesium silicates and by the infilling of shrinkage pores generated during the dehydration of these gels (Carramal et al. 2022).

Dolomite development also reflects strong compositional controls, as evidenced by the frequent occurrence of crystal zoning (Fig. 4H). These features indicate formation under fluctuating physicochemical conditions during eodiagenesis and early mesodiagenesis (Saller et al. 2016; Carvalho et al. 2022; Menezes et al. 2025). The preservation of these compositional heterogeneities throughout burial suggests incomplete or selective recrystallization (Menezes et al. 2025), favoring the localized development of intracrystalline porosity associated with specific compositional bands within dolomite crystals. In addition, partial replacement of dolomite by calcite was recognized (Fig. 3F), providing evidence for dedolomitization processes previously described by Carvalho and Fernandez (2021).

5.1.3 Silica

Silicification represents one of the main diagenetic controls on the petrophysical heterogeneity of the Barra Velha Formation reservoirs (Fig. 5). This spatially heterogeneous and multiphase process exerts contrasting effects on reservoir quality, promoting both porosity reduction through pervasive cementation and secondary porosity

generation associated with silica dissolution and remobilization during burial (Basso et al. 2020; De Jesus et al. 2023; Cembrani et al. 2026).

Cryptocrystalline silica is widely associated with early eodiagenetic conditions and is thought to have formed through two main pathways: (i) replacement of unstable magnesium clay minerals and primary constituents and (ii) syndepositional to bioinduced precipitation within microbial systems (Tosca and Wright 2015; Altenhofen et al. 2024; Gomes et al. 2025; Castro et al. 2026). These processes account for its occurrence in both spherulitestones and microbialites, and indicate a primary control exerted by the physicochemical conditions of the early lacustrine system (Tosca and Wright 2015; Sartorato 2018; Castro et al. 2026).

Silicification by microcrystalline quartz and chalcedony has traditionally been linked to the eodiagenetic replacement of magnesium clay minerals and primary constituents (Herlinger et al. 2017; Carramal et al. 2022; Menezes et al. 2025; Cembrani et al. 2026), although part of these phases has also been attributed to burial-related and hydrothermal processes (Lima et al. 2020; Rochelle-Bates et al. 2022). The strong spatial association between silicification and stylolites, together with the recurrent occurrence of both micro- and macrocrystalline silica (Fig. 5E and 7B), suggests that these phases are genetically linked to silica-rich fluid circulation along pressure-solution surfaces. In this context, stylolites likely acted as major conduits for silica-bearing basinal fluids during burial, promoting both replacement of the carbonate framework and silica cementation. These relationships indicate that a significant proportion of silicification in the Barra Velha Formation cannot be attributed exclusively to eodiagenetic processes, but also reflects burial-related episodes during which pressure dissolution and chemical compaction promoted silica generation, remobilization, and redistribution.

Megaquartz, also referred to as macrocrystalline silica or mosaic quartz, is widely associated with late diagenetic stages linked to deep burial and hydrothermal fluid circulation (Corrêa et al. 2025; Cembrani et al. 2026). This phase occurs predominantly as a pore-filling cement within vuggy porosity, dissolution channels, and fractures, although it is also locally preserved within remnant primary pore systems (Fig. 5B; Brito et al. 2024; Matheus et al. 2025; Menchick et al. 2026). Its close association with saddle dolomite, barite, celestine, and fracture networks further supports precipitation from hydrothermal fluids during advanced stages of burial, reinforcing the role of hydrothermal circulation in the late diagenetic evolution of the Barra Velha Formation (Fig. 6A).

The concentration of megaquartz adjacent to fault zones and structural highs indicates a strong structural control on the migration of silica-rich fluids and the development of late-stage silicification (Fig. 1D; Herlinger et al. 2017; Basso et al. 2020; Lima et al. 2020; Leite et al. 2025; Cembrani et al. 2026). In the Mero Field, the abundance of igneous intrusions documented by Martins et al. (2025), together with the presence of a thick igneous interval directly underlying the studied succession, suggests an important magmatic contribution to the generation of these fluids (Corrêa et al. 2025; Cembrani et al. 2026). Nevertheless, the recurrent association between stylolites and megaquartz precipitation, similar to that observed for late-stage microcrystalline quartz, also indicates significant silica remobilization during burial, with stylolites acting as preferential pathways for the circulation of heated basinal fluids.

The occurrence of discontinuous syntaxial overgrowths overlain by drusy and comb quartz cements, commonly displaying a palisade habit oriented toward intergranular pore space, indicates early silica precipitation during the initial stages of burial, contributing to the partial preservation of porosity in hybrid sandstones (Fig. 5D; Houseknecht 1987; Wang et al. 2021; Castro et al. 2023). Corroded surfaces on detrital

quartz grains in contact with these cements suggest early quartz dissolution associated with the circulation of alkaline fluids (Pye and Krinsley 1985; McBride 1989). In contrast, lobate to sutured contacts between detrital quartz grains record pressure dissolution during more advanced burial stages (Fig. 7D; Land et al. 1987; Houseknecht 1988; Wang et al. 2021), promoting local silica remobilization and subsequent quartz cementation.

These relationships indicate that, in addition to silica derived from the dissolution of magnesium clay minerals and hydrothermal sources widely recognized in the Barra Velha Formation (Gomes et al. 2020; Cembrani et al. 2026), quartz-rich intervals acted as important internal sources of silica within the diagenetic system. Chemical dissolution of detrital quartz likely represented a significant source of dissolved silica during burial, contributing to its redistribution throughout the succession. The combined effects of heated alkaline fluids and pressure-solution processes promoted silica release, remobilization, and late-stage precipitation, both locally and in more distal sectors of the diagenetic system (Schwartzentruber et al. 1987; Sheldon et al. 2003; van Noort et al. 2008; Oye et al. 2018, 2020; Castro et al. 2023).

5.1.4 Accessory Minerals

Accessory minerals such as barite, Sr-rich barite, celestine, and pyrite occur predominantly as pore-filling phases within vuggy porosity and fractures, and locally replace pre-existing diagenetic minerals (Fig. 6). Their occurrence defines mineral assemblages commonly associated with hydrothermal systems developed during deep burial (Herlinger et al. 2017; Basso et al. 2020; Lima et al. 2020). The preferential distribution of these phases along fractures and fluid-flow pathways supports a late-stage origin linked to hydrothermal fluid circulation (Basso et al. 2020; Lima et al. 2020; Carvalho et al. 2022). Furthermore, their recurrent association with megaquartz and saddle dolomite reinforces the interpretation of hydrothermal episodes responsible for the

remobilization and late precipitation of silica and dolomite within the Barra Velha Formation (Fig. 6D).

In contrast, minerals such as dawsonite record hyperalkaline conditions within hypersaline lacustrine systems influenced by volcanic activity (Farias et al. 2019). These phases have also been linked to the early diagenetic alteration of primary magnesium clay minerals (Tosca and Wright 2015; Carramal et al. 2022; Schrank et al. 2024). This interpretation is consistent with their occurrence in association with partially dolomitized matrices in spherulitestones (Fig. 6C), suggesting a genetic relationship between magnesium clay mineral alteration, dolomitization, and the precipitation of alkaline authigenic minerals during eodiagenesis.

In contrast to these alkaline mineral assemblages, framboidal pyrite is concentrated mainly within organic-rich intervals, particularly microbialites, indicating early precipitation mediated by microbial activity and bacterial sulfate reduction (Castro et al. 2026). Its subordinate occurrence within magnesium clay-rich matrices further suggests that pyrite formation was integrated into the early diagenetic evolution of these deposits and may have accompanied the partial alteration and replacement of unstable magnesium silicates (Fig. 6B; Schrank et al. 2024; Menchick et al. 2026).

5.1.4 Dissolution, Compaction, and Porosity Evolution

The evolution of porosity in the Barra Velha Formation reflects the superposition of mechanical, chemical, and mineralogical processes operating from the earliest stages of diagenesis through deep burial (Fig. 7; Herlinger et al. 2017). The preservation or obliteration of primary porosity was strongly controlled by facies heterogeneity, original mineralogical composition, and the spatial distribution of diagenetic phases (Carvalho et al. 2022; Menchick et al. 2026). Evidence of early mechanical compaction includes planar

grain contacts, grain fracturing, and deformation of peloids and micritic components (Fig. 7A). With progressive burial, chemical compaction became increasingly important and is recorded by the development of lobate and serrated contacts, dissolution seams, and stylolites, indicating pressure dissolution and mass redistribution throughout the carbonate framework (Fig. 7C).

The dissolution of depositional magnesium clay minerals and their early replacement by dolomite played a fundamental role in the local preservation of interparticle porosity and in the generation of microporosity associated with contraction and dehydration of the original matrix (Fig. 4 C – D; Herlinger et al. 2023; Schrank et al. 2024). However, progressive dolomitization, coupled with mesodiagenetic recrystallization and chemical compaction, increasingly promoted fabric obliteration and reduced pore connectivity (Fig. 4F). Similarly, eo- to mesodiagenetic silicification acted predominantly as a cementation process, contributing to the progressive occlusion of both primary and secondary pore systems (Fig. 5). In contrast, late-stage hydrothermal fluid circulation commonly induced dissolution of the carbonate framework, generating vuggy porosity and promoting silica remobilization, which was subsequently precipitated as megaquartz within fractures, dissolution conduits, and residual secondary porosity (Lima et al. 2020; Corrêa et al. 2025; Cembrani et al. 2026). Collectively, these processes indicate a strongly multistage porosity evolution governed by the interplay among primary mineralogical composition, progressive diagenetic reorganization, and episodic fluid circulation during burial.

5.1.5 Integrated Paragenetic Evolution

The diagenetic evolution of the Barra Velha Formation reflects the superposition of multiple processes operating from eodiagenesis to advanced burial stages, including carbonate recrystallization, dolomitization, silicification, mechanical and chemical

compaction, and episodic hydrothermal fluid circulation (Fig. 8) The spatial and temporal distribution of these phases indicates strong control by primary mineralogical composition, facies heterogeneity, and structural reactivation throughout basin evolution.

The earliest diagenetic stages were dominated by recrystallization of primary calcite, dissolution of magnesium silicates, and precipitation of calcite, blocky dolomite, and cryptocrystalline silica. These processes developed under alkaline and highly evaporative conditions, favoring intense interaction between depositional magnesium silicates and pore fluids. Partial dissolution of these phases also contributed to the release of Mg and Si into the diagenetic system and promoted the generation of secondary porosity.

With progressive burial, chemical compaction became increasingly important, promoting pervasive recrystallization, stylolite development, and silica remobilization. During this stage, blocky dolomite evolved toward mosaic textures through progressive recrystallization, while silicification became increasingly concentrated along stylolites, fractures, and other preferential fluid-flow pathways.

Late-stage diagenesis was marked by hydrothermal fluid circulation associated with tectonic reactivation and regional magmatism. These events promoted the precipitation of megaquartz, saddle dolomite, sulfates, and sulfides, together with extensive recrystallization and localized dissolution of the carbonate framework. The concentration of these mineral assemblages along faults, fractures, and stylolitic zones highlights the fundamental role of structural conduits in controlling fluid migration and the redistribution of diagenetic products throughout the succession.

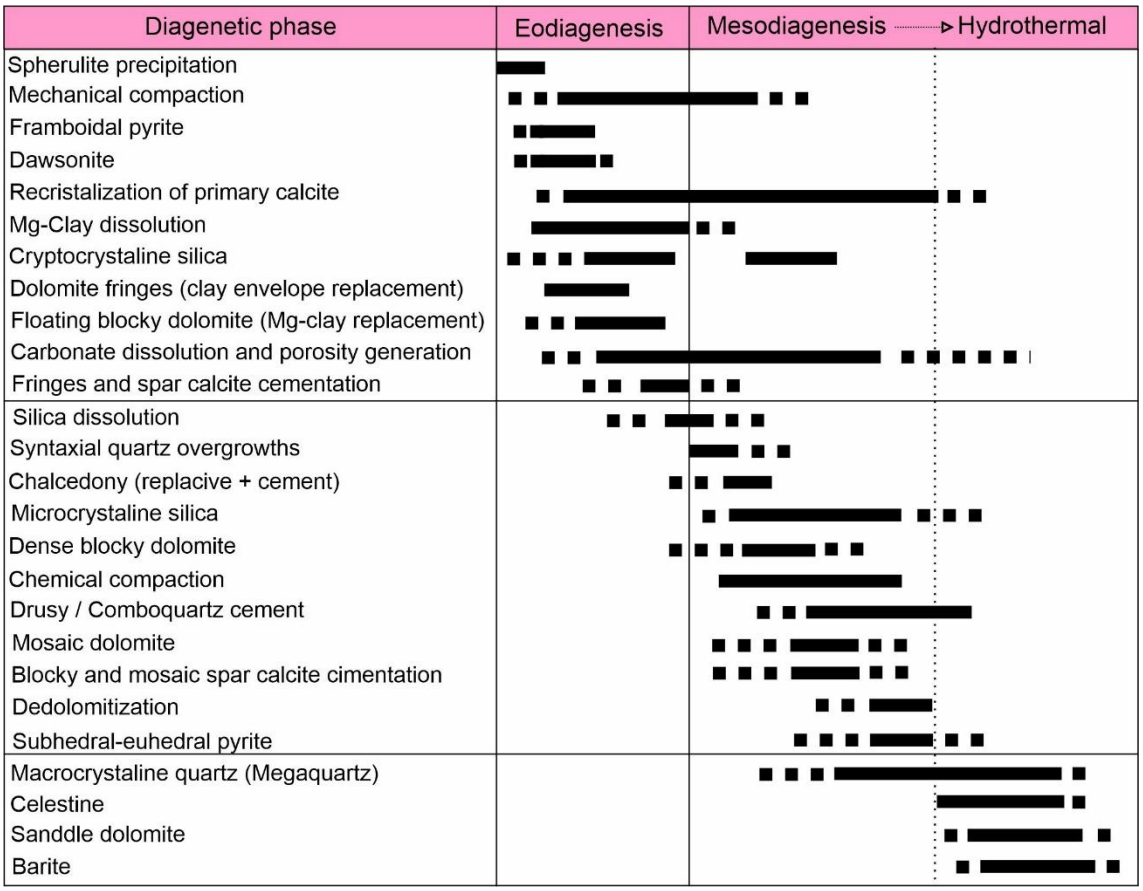

Figure 8 - Paragenetic framework illustrating the relative timing of the principal diagenetic processes and mineral phases recognized in the studied interval, including eodiagenetic, mesodiagenetic, and hydrothermal events.

Ultimately, reservoir quality in the Barra Velha Formation reflects the interplay between depositional inheritance and multistage diagenetic modification. Facies architecture and primary mineralogy controlled the distribution of reactive phases and pore networks, influencing subsequent recrystallization, dolomitization, silicification, dissolution, and cementation. Burial compaction and structurally controlled hydrothermal fluid circulation further modified the reservoir through mineral redistribution, porosity occlusion, and localized enhancement. These results demonstrate that reservoir quality in alkaline lacustrine carbonates is governed by the coupled effects of depositional heterogeneity, mineralogical composition, and evolving diagenetic fluid systems. Although focused on

the Barra Velha Formation, the documented paragenetic framework provides broader insights into fluid–rock interaction, mineral replacement, and porosity evolution in analogous lacustrine carbonate reservoirs characterized by complex mineral assemblages and multistage diagenetic histories.

6. **Conclusion**

The diagenetic evolution of the Barra Velha Formation in the Mero Field reflects the interaction among depositional architecture, primary mineralogy, burial processes, and structurally controlled fluid flow, which collectively governed diagenetic phase distribution and reservoir heterogeneity. The main conclusions are as follows:

1. Facies heterogeneity and primary mineralogical composition exerted first-order controls on dolomitization, silicification, fluid circulation, and porosity preservation throughout burial.
2. Replacement of depositional magnesium clay minerals represents the main mechanism of early dolomitization and a major source of Mg and Si for the diagenetic system. Preservation of magnesium silicate relics and dawsonite occurrence indicate that early diagenesis was strongly influenced by hypersaline and hyperalkaline lacustrine conditions.
3. Different replacive dolomite varieties record the progressive evolution of a dolomitization system, from early replacement of magnesium clay minerals to burial-related fabric modification and recrystallization. A later dolomite phase reflects deep-burial precipitation from evolved basinal fluids.
4. Silicification resulted from multiple diagenetic episodes involving silica derived from magnesium clay alteration, hydrothermal fluids, and internal redistribution from quartz-rich intervals. Stylolite zones acted as important pathways for silica

remobilization and fluid circulation, promoting carbonate replacement and late quartz precipitation.

5. Late-stage minerals, including megaquartz, saddle dolomite, barite, celestine, and pyrite, associated with faults, fractures, and stylolites, record burial-related fluid circulation. Together with dissolution, chemical compaction, and recrystallization, these processes controlled the multistage evolution of porosity and reservoir heterogeneity.

Despite these advances, constraining the composition and evolution of diagenetic fluids and the timing of mineral transformations requires complementary approaches, including isotopic analyses, fluid inclusions, and XRD investigations.

Acknowledgements

This research was conducted within the ANP-funded R&D project "Impact of tectono-stratigraphic controls on Pre-salt reservoir quality and distribution" (ANP No. 23009-4), developed through the UFRJ–Shell Brasil partnership. We thank the PRESAL Project team and LAGESED/UFRJ for technical support and constructive discussions.

Disclosure statement

The authors declare that they have no known competing financial interests or personal relationships that could have appeared to influence the work reported in this paper.

Data availability statement

The data that support the findings of this study are available from the corresponding author, [A. P. de Castro], upon reasonable request.

Author contributions: CRediT

Conceptualization, data curation, Formal analysis, writing (A.P. De Castro); Supervision, validation, visualization (J. Oste); Supervision, Project administration, Funding acquisition (L. Borghi).

References

Adriano MS, Figueiredo JP, Coelho PHGR, Borghi L (2022) Tectonic and stratigraphic evolution of the Santos Basin rift phase: New insights from seismic interpretation on Tupi oil field area. J South Am Earth Sci 116:103842.

Altenhofen SD, Rodrigues AG, Borghi L, De Ros LF (2024) Dynamic re-sedimentation of lacustrine carbonates in the Búzios Field, pre-salt section of Santos Basin, Brazil. J South Am Earth Sci 138:104863. https://doi.org/10.1016/j.jsames.2024.104863

Altenhofen SD, Borghi L, De Ros LF, Rodrigues AG (2026) Internal solitons as a mechanism for reworking lacustrine carbonates: A case study from the Aptian Barra Velha Formation, Santos Basin, Brazil. Pet Geosci 32:petgeo2025-074.

Alves TM, Fetter M, Lima C, Cartwright JA, Cosgrove J, Gangá A, Queiroz CL, Strugale M (2017) An incomplete correlation between pre-salt topography, top reservoir erosion, and salt deformation in deep-water Santos Basin (SE Brazil). Mar Petrol Geol 79:300–320. https://doi.org/10.1016/j.marpetgeo.2016.10.015

Agência Nacional do Petróleo, Gás Natural e Biocombustíveis (ANP) (2021) *Boletim da Produção de Petróleo e Gás Natural*, No. 136. ANP, Rio de Janeiro.

Araújo CC, Madrucci V, Homewood P, Mettraux M, Ramnani CW, Spadini AR (2022) Stratigraphic and sedimentary constraints on presalt carbonate reservoirs of the

South Atlantic Margin, Santos Basin, offshore Brazil. AAPG Bull 106:2513–2546. https://doi.org/10.1306/08082219218

Armelenti G, Goldberg K, Kuchle J, De Ros LF (2016) Deposition, diagenesis and reservoir potential of non-carbonate sedimentary rocks from the rift section of Campos Basin, Brazil. Pet Geosci 22:223–239. https://doi.org/10.1144/petgeo2015-035

Azerêdo AC, Duarte LV, Silva AP (2021) The challenging carbonates from the Pre-Salt reservoirs offshore Brazil: Facies, palaeoenvironment and diagenesis. J South Am Earth Sci 108:103202. https://doi.org/10.1016/j.jsames.2021.103202

Basso M, Belila AMP, Chinelatto GF, Souza JPDP, Vidal AC (2020) Sedimentology and petrophysical analysis of pre-salt lacustrine carbonate reservoir from the Santos Basin, southeast Brazil. Int J Earth Sci 110:2573–2595. https://doi.org/10.1007/s00531-020-01932-7

Blair TC, McPherson JG (1999) Grain-size and textural sorting characteristics of gravelly sediments in high-energy sedimentary environments. J Sediment Res 69:6–19.

Brito JPS, Santos RV, Gonçalves GO, Barbosa PF, Souza Cruz CE, Ushirobira CA, Souza VS, Richter FM, Abreu CJ (2024) U-Pb dating of Barra Velha carbonates reveals the influence of Santos Basin sedimentary and tectonothermal history on pre-salt carbonate ages. Mar Petrol Geol 168:107035.

Buckley JP, Bosence DWJ, Elders CF (2015) Tectonic setting and stratigraphic architecture of an Early Cretaceous lacustrine carbonate platform, Sugar Loaf High, Santos Basin, Brazil. In: Bosence DWJ, Gibbons KA, Le Heron DP, Morgan WA, Pritchard T, Vining BA (eds) *Microbial carbonates in space and time: Implications for global exploration and production*. Geol Soc Lond Spec Publ 418:175–191. https://doi.org/10.1144/SP418.13

Cainelli C, Mohriak W (1999) Some remarks on the evolution of sedimentary basins. Episodes 22:206–216.

Carlotto MA, Silva RCB, Yamato AA, Trindade WL, Moreira JLP, Fernandes RARA, Ribeiro OJS, Gouveia Jr WP, Carminati JP, Qicai D, Junfeng Z, Silva-Teles Jr AC et al (2017) Libra: A newborn giant in the Brazilian pre-salt province. In: Merrill RK, Sternbach CA (eds) *Giant Fields of the Decade 2000–2010*. AAPG Memoir 113:165–176. https://doi.org/10.1306/13572006M1133685

Carminatti M, Wolff B, Gamboa LAP (2008) New exploratory frontiers in Brazil. In: 19th World Petroleum Congress, Madrid.

Carramal NG, Oliveira DM, Cacela ASM, Cuglieri MAA, Rocha NP, Viana SM, Toledo SLV, Pedrinha S, De Ros LF (2022) Paleoenvironmental insights from the deposition and diagenesis of Aptian pre-salt magnesium silicates from the Lula Field, Santos Basin, Brazil. J Sediment Res 92:12–31.

Carvalho MD, Fernandes FL (2021) Pre-salt depositional system: Sedimentology, diagenesis, and reservoir quality of the Barra Velha Formation, as a result of the Santos Basin tectono-stratigraphic development. In: Mello MR, Yilmaz PO, Katz BJ (eds) *The Supergiant Lower Cretaceous Pre-Salt Petroleum Systems of the Santos Basin, Brazil*. AAPG Memoir 124:121–154. https://doi.org/10.1306/13732337msb.5.1708

Carvalho AMA, Hamon Y, De Souza Jr OG, Carramal NG, Collard N (2022) Facies and diagenesis distribution in an Aptian pre-salt carbonate reservoir of the Santos Basin, offshore Brazil: A comprehensive quantitative approach. Mar Petrol Geol 141:105708. https://doi.org/10.1016/j.marpetgeo.2022.105708

Castro AP, Guedes CCF, Vesely FF, Silveira DM, Neves LF (2023) Provenance, diagenesis and reservoir quality of sandstone facies of the Maracangalha Formation,

Recôncavo Basin, northeastern Brazil. Mar Petrol Geol 158. *(Adicionar número do artigo e DOI, se disponível.)*

Castro AP, Oste JF, Souza JT, Guedes C, Borghi L (2025) Microbialites and biosignatures in the Barra Velha Formation, Santos Basin, Brazil. Submitted to Geomicrobiol J.

Castro AP, Oste JF, Silva WJ, Borghi L (2026) Facies architecture and REE+Y constraints on the evolution of a rift-related lacustrine carbonate system (Lower Cretaceous, Santos Basin, SE Brazil). SSRN. https://doi.org/10.2139/ssrn.6485089

Cembrani E, Schmidt J, Souza M, Santos T, Schrank ABS, Freitas W, Maraschin A, Barili R, Rodrigues AG, De Ros LF (2026) Multi-stage silicification in the Aptian pre-salt reservoirs of the Santos Basin, Brazil: Lacustrine recirculation and hydrothermal processes of silica precipitation in continental carbonates. J Sediment Res 96:41–64.

Chang HK, Kowsmann RO, Figueiredo AMF, Bender A (1992) Tectonics and stratigraphy of the East Brazil Rift system: An overview. Tectonophysics 213:97–138. https://doi.org/10.1016/0040-1951(92)90253-3

Chang HK, Assine ML, Corrêa FS, Tinen JS, Vidal AC, Koike L (2008) Sistemas petrolíferos e modelos de acumulação de hidrocarbonetos na Bacia de Santos. Rev Bras Geociênc 38:29–46. https://doi.org/10.25249/0375-7536.2008382s2946

Choquette PW, Pray LC (1970) Geologic nomenclature and classification of porosity in sedimentary carbonates. AAPG Bull 54:207–250.

Corrêa RSM, Carvalho B, Ukar E, Laubach SE, Pestilho ALS, Fall A, Larson T, Stockli DF, Stockli LD, Lüders V, Niedermann S, Banks DA (2025) Brittle deformation and hydrothermal alteration in the Barra Velha Formation, Santos Basin, offshore Brazil. AAPG Bull 109:545–590.

Davison I (2007) Geology and tectonics of the South Atlantic Brazilian salt basins. Geol Soc Lond Spec Publ 272:345–359. https://doi.org/10.1144/GSL.SP.2007.272.01.18

De Jesus IL, Abrantes Jr FR, Ferreira DJA, Lupinacci WM (2023) Carbonate reservoir quality and permoporosity obliteration due to silicification processes in the Barra Velha Formation, Santos Basin, southeastern Brazil. Braz J Geol 53:e20220086.

De Ros LF, Oliveira DM (2023) An operational classification system for the South Atlantic pre-salt rocks. J Sediment Res 93:693–704.

Dravis JJ (1991) Carbonate petrography—Update on new techniques and applications. J Sediment Res 61(4):626-629.

Dravis JJ, Yurewicz DA (1985) Enhanced carbonate petrography using fluorescence microscopy. J Sediment Res 55:795–804. https://doi.org/10.1306/212F8800-2B24-11D7-8648000102C1865D

Farias F, Szatmari P, Bahniuk A, Franca AB (2019) Evaporitic carbonates in the pre-salt of Santos Basin: Genesis and tectonic implications. Mar Petrol Geol 105:251–272. https://doi.org/10.1016/j.marpetgeo.2019.04.020

Gomes PO, Parry J, Martins W (2002) The outer high of the Santos Basin, southern São Paulo Plateau, Brazil: Tectonic setting, relation to volcanic events and some comments on hydrocarbon potential. In: AAPG Hedberg Conference on the Hydrocarbon Habitat of Volcanic Rifted Passive Margins, Stavanger.

Gomes JP, Bunevich RB, Tedeschi LR, Tucker ME, Whitaker FF (2020) Facies classification and patterns of lacustrine carbonate deposition of the Barra Velha Formation, Santos Basin, Brazilian pre-salt. Mar Petrol Geol 113:104176. https://doi.org/10.1016/j.marpetgeo.2019.104176

Gomes AS, Vasconcelos PM (2021) Geochronology of the Paraná-Etendeka large igneous province. Earth-Sci Rev 220:103716.

Gomes JPB, Bunevich RB, Sartorato ACL, Tedeschi LR, Tonietto SN, Tucker ME, Whitaker F (2025) Early diagenetic evolution based on petrography and stable isotope analysis in the Barra Velha Formation of the Brazilian pre-salt. Depos Rec 11:70–94. https://doi.org/10.1002/dep2.288

Herlinger R, Zombonato EE, De Ros LF (2017) Influence of diagenesis on the quality of Lower Cretaceous pre-salt lacustrine carbonate reservoirs from northern Campos Basin, offshore Brazil. J Sediment Res 87:1285–1313. https://doi.org/10.2110/jsr.2017.70

Herlinger Jr R, De Ros LF, Surmas R, Vidal A (2023) Residual oil saturation investigation in Barra Velha Formation reservoirs from the Santos Basin, offshore Brazil: A sedimentological approach. Sediment Geol 448:106372.

Hiatt EE, Pufahl PK (2014) Cathodoluminescence petrography of carbonate rocks: A review of applications for understanding diagenesis, reservoir quality and pore system evolution. Short Course 45:75–96.

Houseknecht DW (1987) Assessing the relative importance of compactional processes and cementation to the reduction of porosity in sandstones. AAPG Bull 71:633–642.

Houseknecht DW (1988) Intergranular pressure solution in four quartzose sandstones. J Sediment Petrol 58:228–246.

Jácomo MH, Hartmann GA, Rebelo TB, Mattos NH, Batezelli A, Leite EP (2023) Mineralogical modeling and petrophysical properties of the Barra Velha Formation,

Santos Basin, Brazil. Petrophysics 64:518–543. https://doi.org/10.30632/PJV64N4-2023a3

Land LS, Milliken KL, McBride EF (1987) Diagenetic evolution of Cenozoic sandstones, Gulf of Mexico sedimentary basin. Sediment Geol 50:195–225.

Leite M, Reis H, Fonte Boa T, Moura Costa F, Gonçalves Costa DF (2025) The Alto de Tupi: A structural long-lasting high and its control on the Aptian pre-salt successions of the Santos Basin, Brazil. J South Am Earth Sci 166:105733.

Lima BEM, De Ros LF (2019) Deposition, diagenetic and hydrothermal processes in the Aptian pre-salt lacustrine carbonate reservoirs of the northern Campos Basin, offshore Brazil. Sediment Geol 383:55–81. https://doi.org/10.1016/j.sedgeo.2019.01.006

Lima BEM, Tedeschi LR, Pestilho ALS, Santos RV, Vasquez JC, Guzzo JVP, De Ros LF (2020) Deep-burial hydrothermal alteration of the pre-salt carbonate reservoirs from northern Campos Basin, offshore Brazil: Evidence from petrography, fluid inclusions, Sr, C and O isotopes. Mar Petrol Geol 113:104143. https://doi.org/10.1016/j.marpetgeo.2019.104143

Machel HG (2000) Application of cathodoluminescence to carbonate diagenesis. In: Pagel M, Barbin V, Blanc P, Ohnenstetter D (eds) *Cathodoluminescence in Geosciences*. Springer, Berlin, Heidelberg, pp 271–301.

Manzo E, Perri E, Tucker ME (2012) Carbonate deposition in a fluvial tufa system: Processes and products (Corvino Valley, southern Italy). Sedimentology 59:553–577. https://doi.org/10.1111/j.1365-3091.2011.01265.x

Marins GM, Abrantes F, Oliveira L (2025) Seismic interpretation of the Mero Field igneous rocks and its implications for pre- and post-salt CO2 generation, Santos

Basin, offshore Brazil. Mar Petrol Geol 174:107291. https://doi.org/10.1016/j.marpetgeo.2025.107291

Matheus GF, Basso M, Mendes L, Winter A, Medeiros RSP, Souza JPP, Chinelatto GF, Camargo MM, Vidal AC (2025) Integrated multiscale pore characterization of carbonate rocks in the Barra Velha Formation, Santos Basin, Brazil. SPE J. 30(08):4741-4764. https://doi.org/10.2118/228310-PA.

McBride EF (1989) Quartz cement in sandstones: A review. Earth-Sci Rev 26:69–112.

Menchick M, Cunha RB, Rodrigues AG, De Ros LF (2026) Reservoir petrofacies and diagenetic evolution of the Aptian Barra Velha Formation, Santos Basin, Brazil. Research Square (preprint). https://doi.org/10.21203/rs.3.rs-9089991/v1

Menezes MN, Dal' Bó PF, Smith JJ, Mattos NH, Ribeiro C, Arena M, Santos HN, Pires GLC, Watahe P, Borghi L (2025) The influence of diagenetic conditions and fault zones on karstification development in the Barra Velha Formation (Aptian, Santos Basin, Brazil). Mar Petrol Geol 178:107427.

Mercedes-Martín R, Ayora C, Tritlla J, Sánchez-Román M (2019) The hydrochemical evolution of alkaline volcanic lakes: A model to understand the South Atlantic pre-salt mineral assemblages. Earth-Sci Rev 198:102938.

Milani EJ, Brandão JASL, Zalán PV, Gamboa LAP (2000) Petróleo na margem continental brasileira: Geologia, exploração, resultados e perspectivas. Rev Bras Geofís 18:351–396. https://doi.org/10.1590/S0102-261X2000000300012

Mohriak W, Nemčok M, Enciso G (2008) South Atlantic divergent margin evolution: Rift-border uplift and salt tectonics in the basins of SE Brazil. Geol Soc Lond Spec Publ 294:365–398. https://doi.org/10.1144/SP294.19

Moreira JLP, Madeira CV, Gil JA, Machado MAP (2007) Bacia de Santos. Bol Geociênc Petrobras 15:531–549.

Oye OJ, Aplin AC, Jones SJ, Gluyas JG, Bowen L, Orland IJ, Valley JW (2018) Vertical effective stress as a control on quartz cementation in sandstones. Mar Petrol Geol 98:640–652.

Oye OJ, Aplin AC, Jones SJ, Gluyas JG, Bowen L, Harwood J, Orland IJ, Valley JW (2020) Vertical effective stress and temperature as controls of quartz cementation in sandstones: Evidence from North Sea Fulmar and Gulf of Mexico Wilcox sandstones. Mar Petrol Geol 115:104289.

Pagel M, Barbin V, Blanc P, Ohnenstetter D (2000) An introduction. In: Pagel M, Barbin V, Blanc P, Ohnenstetter D (eds) *Cathodoluminescence in Geosciences*. Springer, Berlin, Heidelberg, pp 1–21. https://doi.org/10.1007/978-3-662-04086-7_1

Pye K, Krinsley DH (1985) Formation of secondary porosity in sandstones by quartz framework grain dissolution. Nature 317:54–56.

Pozzi RPC, Fernandes RAR, Silva RCB, Oliveira LC, Sartorato ACL, Figueiredo Junior FP, Penatti APR, Rancan CC, Cruz FEG, Carlotto MA, Mizuno TA, Oliveira VC (2024) Campo de Mero: caracterização dos reservatórios e desenvolvimento da produção. In: Chagas AAP, Araújo CD, Santos LA (eds) *As Grandes Descobertas do Pré-Sal no Atlântico*. Petrobras, Rio de Janeiro, pp 884–945.

Rebelo TB, Batezelli A, Mattos NH, Leite EP (2023) Sedimentary processes and paleoenvironment reconstruction of the Barra Velha Formation, Santos Basin, Brazilian pre-salt. Mar Petrol Geol 150:106141. https://doi.org/10.1016/j.marpetgeo.2023.106141

Rocha L, Favoreto J, Borghi L (2021) Coquinas da Formação Itapema, Campo de Mero (Pré-sal da Bacia de Santos): Análise de microfácies e paleoambiente deposicional.

Anu Inst Geociênc UFRJ 44:39883. https://doi.org/10.11137/1982-3908_2021_44_39883

Rochelle-Bates N, Wood R, Schröder S, Roberts NMW (2022) In situ U–Pb geochronology of pre-salt carbonates reveals links between diagenesis and regional tectonics. Terra Nova 34:271–277. https://doi.org/10.1111/ter.12586

Rodríguez-Berriguete Á, Dal' Bó PF, Valle B, Borghi L (2022) When distinction matters: Carbonate shrubs from the Aptian Barra Velha Formation of the Brazilian pre-salt. Sediment Geol 440:106236.

Saller A, Rushton S, Buambua L, Inman K, McNeil R, Dickson JT (2016) Pre-salt stratigraphy and depositional systems in the Kwanza Basin, offshore Angola. AAPG Bull 100:1135–1164. https://doi.org/10.1306/02111615216

Sartorato ACL (2018) Caracterização faciológica, estratigráfica e diagenética dos reservatórios carbonáticos da Formação Barra Velha, Bacia de Santos. Dissertation, Universidade do Estado do Rio de Janeiro.

Schrank ABS, Dos Santos T, Altenhofen SD, Freitas W, Cembrani E, Haubert T, Dalla Vecchia F, Barili R, Rodrigues AG, De Ros LF (2024) Interactions between clays and carbonates in the Aptian pre-salt reservoirs of Santos Basin, eastern Brazilian Margin. Minerals 14:191. https://doi.org/10.3390/min14020191

Schwartzenruber J, Furst W, Renon H (1987) Dissolution of quartz into dilute alkaline solutions at 90 °C: A kinetic study. *Geochim Cosmochim Acta* 51(7):1867–1874.

Sheldon HA, Wheeler J, Worden RH, Cheadle MJ (2003) An analysis of the roles of stress, temperature, and pH in chemical compaction of sandstones. *J Sediment Res* 73(1):64–71.

Silva DRL, Terra SA, Ribeiro A, Borghi L (2025) The lower Barra Velha Formation (Aptian) in the Atapu Field, Santos Basin: Geological model for a pre-salt succession. *J South Am Earth Sci* 155:105380. https://doi.org/10.1016/j.jsames.2024.105380

Terra SA, da Silva DRL, Ribeiro A, Borghi L (2023) The lower Barra Velha Formation (Aptian) in the Atapu Field, Santos Basin: Geological model for a pre-salt succession. *J South Am Earth Sci* 131:104589. https://doi.org/10.1016/j.jsames.2023.104589

Tritlla J, Esteban M, Loma R, Mattos A, Sánchez V, Boix C, Vieira de Luca CH, Carballo J, Levresse G (2018) Carbonates that are no more: Silicified pre-salt oil reservoirs in Campos Basin (Brazil). In: *AAPG Annual Convention and Exhibition (ACE)*. AAPG Search and Discovery Article 90323.

Tosca NJ, Wright VP (2015) Diagenetic pathways linked to labile Mg-clays in lacustrine carbonate reservoirs: A model for the origin of secondary porosity in the Cretaceous pre-salt Barra Velha Formation, offshore Brazil. In: Armitage PJ, Butcher AR, Churchill JM, Csoma AE, Hollis C, Lander RH, Omma JE, Worden RH (eds) *Reservoir Quality of Clastic and Carbonate Rocks: Analysis, Modelling and Prediction*. Geological Society, London, Special Publications 435, pp 33–46.

Unternehr P, Péron-Pinvidic G, Manatschal G, Sutra E (2010) Hyper-extended crust in the South Atlantic: In search of a model. *Pet Geosci* 16(3):207–215. https://doi.org/10.1144/1354-079309-843

van Noort R, Spiers CJ, Pennock GM (2008) Compaction of granular quartz under hydrothermal conditions: Controlling mechanisms and grain boundary processes. *J Geophys Res Solid Earth* 113(B1).

Wang Y, Chi G, Li Z, Bosman S (2021) Large-scale thermal convection in sedimentary basins revealed by coupled quartz cementation-dissolution distribution pattern and reactive transport modeling: A case study of the Proterozoic Athabasca Basin (Canada). *Earth Planet Sci Lett* 574:117168.

Wang H, Zhang M, Fan G, Xiao L, Zuo G, Yang L, Pang X, Wang C, Zhang Y (2023) Prediction of lithology in lacustrine carbonates using well logs: The Cretaceous Barra Velha Formation in Santos Basin, offshore Brazil. *Geol J* 58(11):4271–4282.

Wright VP, Barnett AJ (2015) An abiotic model for the development of textures in some South Atlantic Early Cretaceous lacustrine carbonates. In: Bosence DWJ, Gibbons K, Le Heron DP, Morgan WA, Pritchard T, Vining BA (eds) *Microbial Carbonates in Space and Time: Implications for Global Exploration and Production*. Geological Society, London, Special Publications 418, pp 209–219. https://doi.org/10.1144/SP418.3